Predicting resilient modulus of flexible pavement foundation using extreme gradient boosting based optimized models

Reza Sarkhani Benemaran[a], Mahzad Esmaeili-Falak[*b] and Akbar Javadi[c]

[a] *PhD candidate, Department of Civil Engineering, Faculty of Geotechnical Engineering, University of Zanjan, Zanjan, Iran (Orcid:0000-0001-9569-388X)*

[b] *Assistant Professor, Dep. of Civil Engineering, North Tehran Branch, Islamic Azad University, Tehran, Iran (Orcid:0000-0003-3089-8598)*

* Corresponding author, Email: Mahzad.ef@tabrizu.ac.ir

[c] *Professor, Dept. of Engineering, Univ. of Exeter, Exeter, EX4 4QF, UK (Orcid:0000-0001-8376-4652)*

Resilient modulus (M_R) plays the most critical role in the evaluation and design of flexible pavement foundations. M_R is utilized as the principal parameter for representing stiffness and behavior of flexible pavement foundation in experimental and semi-empirical approaches. To determine M_R, cyclic triaxial compressive experiments under different confining pressures and deviatoric stresses are needed. However, such experiments are costly and time-consuming. In the present study, an extreme gradient boosting-based (XGB) model is presented for predicting the resilient modulus of flexible pavement foundations. The model is optimized using four different optimization methods (particle swarm optimization (PSO), social spider optimization (SSO), sine cosine algorithm (SCA), and multi-verse optimization (MVO)) and a database collected from previously published technical literature. The outcomes present that all developed designs have good workability in estimating the M_R of flexible pavement foundation, but the $PSO-XGB$ models have the best prediction accuracy considering both training and testing datasets.

Keywords: Resilient modulus prediction; Artificial neural networks; Extreme gradient boosting; PSO; MVO; SSO; SCA

Introduction

Cohesion-less granular soils are the most common materials used as flexible pavement foundations. A flexible pavement foundation is consists of subgrade, sub-base, and base layers (down to top) in which resilient modulus (M_R) calculates for the subgrade layer, commonly. According to the semi-empirical approaches presented by the Mechanistic-Empirical Pavement Design Guide (MEPDG) and American Association of State Highway and Transportation Officials (AASHTO), resilient modulus (M_R) is the most influential input parameter for modeling the deformation of flexible pavement foundations (AASHTO 2003, PDG 2004). To decrease the thickness of the pavement foundation (subbase and subgrade) and the construction cost, accurate determination of the mechanical properties (including M_R) of these layers through experimental studies is essential (Esmaeili-Falak et al., 2020; Esmaeili-Falak et al., 2017, 2018; Poorjafar et al., 2021; Benemaran et al., 2020; Bardhan et al., 2021; Corrêa-Silva et al., 2021; G. Han et al., 2021; Lee et al., 2021; Lei et al., 2021; L. Liu et al., 2021). The value of M_R represents the rigidity of the pavement foundation materials that show an elastoplastic behavior under traffic loading and various environmental conditions (AASHTO 2003). The most common method to determine M_R is through cyclic triaxial shear tests, with different confining pressures and deviatoric stresses. These tests are complex, costly, and time-consuming and require experienced operators. Another approach for determining M_R of pavement foundations is through forecasting models based on soft computing procedures (de Freitas et al., 2020; Z. Han & Vanapalli, 2016; S. Liu et al., 2016; Ghanizadeh & Tavana Amlashi, 2018; Khasawneh, 2005; Nazzal & Mohammad, 2010; Ozsahin & Oruc, 2008; Pourtahmasb et al., 2015; Shafabakhsh & Tanakizadeh, 2015). In general, the forecasting approaches for determining M_R can be divided into two main categories. The first category includes the approaches that use correlations

between resilient modulus and various physical and mechanical properties (such as P#200, PI, LL, S_r, q_u, ω_{opt}, ω_c, σ_o, and σ_d) (Heukelom and Klomp 1962, Asphalt Institute 1982, Rahim 2005, Kumar *et al.* 2014). The second category includes the forecasting approaches that use stress state (Nazzal and Tatari 2013, Titi and Matar 2018). The stress based approaches to determine M_R for flexible pavement foundations use stress parameters such as confining pressure, deviatoric stress, bulk stress, or combination of them (Barksdale et al., 1997; Dunlap, 1963; Huang, 1993; Moossazadeh & Witczak, 1981; Ni et al., 2020; Seed et al., 1962; Uzan, 1985). An outline of the previous studies on predicting the M_R of flexible pavement foundations is summarized in Table 1.

Sadrossadat et al. presented a model based upon linear genetic programming to estimate the M_R of flexible pavement foundations. For this purpose, they proposed a model that specifies the M_R as a function of the characteristics of the road subgrade and the created stress states using a dataset consisting of various experimental results (Sadrossadat *et al.* 2018). These tests were conducted on cohesive soil samples taken from Ohio, USA, which is classified as A-6 in the AASHTO classification system. To assess the precision and reliability of the developed model, different model performance evaluation indices were assessed. In this study, passing percent of No. 200 sieve, liquid limit, plasticity index, optimum water content, natural water content, saturation degree, uniaxial strength, confining pressure, and deviatoric stress were considered as input variables to predict M_R as the output. Comprising the measured and predicted values showed a good agreement with R^2 values of 0.846, 0.865, 0.810, and 0.865 for all data, training data, validation data, and testing data, respectively.

Ghorbani et al. developed a hybrid artificial neural network (ANN) model optimized by a genetic algorithm (GA) to predict the resilient modulus of flexible

pavement foundations (Ghorbani *et al.* 2020). For this purpose, a dataset including the cyclic triaxial test results and the physical and mechanical properties of the flexible pavement foundation material was considered as input parameters (i.e., $\mathrm{P\#200, PI, LL,}\ \sigma_o,\ \sigma_d,\ S_r, \omega_{opt}, \omega_c,\ and\ \ q_u$). The Genetic algorithm was used to optimize the weights and the bias of the $ANN-GA$ hybrid model. The predicted values were validated and verified against the measured amounts considering various model performance evaluation indices. Finally, a sensitivity analysis was conducted on the variables to assess the generality and effectiveness of the different used parameters. The results demonstrated that both GA and $ANN-GA$ approaches could meticulously estimate the value of M_R of flexible pavement foundation (R^2= 0.97 and 0.87 for $ANN-GA$ and GA models, respectively).

In another study, Kayadelen et al. (2021) employed M5P-tree and Random Forest regression approaches to predict M_R (Kayadelen *et al.* 2021). A numerical model was also used to evaluate the influence of soil parameters on the strain characteristics of the pavement foundation subjected to cyclic loading. A large dataset from different studies was used to build the model. The dataset included soil properties like optimum water content, natural water content, dry unit weight, degree of saturation, uniformity coefficient, percent passing No. 200 sieve, plasticity index, unconfined compressive strength, confining stress, and deviator stress that were used as the input variables against the M_R as the output. The model performance evaluation indices were assessed comprehensively using correlation coefficient (R), root mean square error ($RMSE$), mean absolute error (MAE), root relative squared error ($RRSE$), and relative absolute error (RAE). The results showed that the developed model's outputs are in reasonable agreement with the calculated and predicted values of M_R. The results also showed that the Random Forest model was more accurate than the M5P-tree model.

Heidarabadizadeh et al. employed a hybrid support vector machine using colliding bodies optimization algorithm ($SVM - CBO$) to predict the resilient modulus of granular pavement foundation (Heidarabadizadeh *et al.* 2021). A database was collected from published research that included specific data from various project sites. They used 75% of the data for training and 25% for testing the model. The input parameters used were confining pressure, deviatoric stress, dry unit weight, uniformity coefficient, curvature coefficient, and percent passing a No. 200 sieve and M_R was the output. The R^2 values were about 0.972 to 0.988 for the testing data, which show that the $SVM - CBO$ hybrid model was able to predict the resilient modulus of the pavement foundations with good accuracy.

Enhancing the accuracy of prediction models of M_R is still a major concern in this field of research. A review of the literature shows that most of the research works on predicting M_R have used artificial intelligence models in single or hybrid forms. Also, some traditional model performance evaluation indices have been used in the literature, while new indices have been neglected. In the present study, four extreme gradient boosting based (XGB) hybrid models are used to predict the resilient modulus of granular pavement foundations. These models include particle swarm optimization (PSO), social spider optimization (SSO), sine cosine algorithm (SCA), and multi-verse optimization (MVO) algorithms. The models are developed using a comprehensive dataset, including passing through No. 200 sieve, plasticity index, liquid limit, confining pressure, deviatoric stress, degree of saturation, optimum water content, natural water content, and unconfined compressive strength. In addition to the classic model performance evaluation indices like $RMSE, MAE$, etc., new indices such as $A_{10-\text{index}}$ and VAF are employed to assess the efficiency of the developed models. The

effectiveness of the model performance indices for the developed models is evaluated comprehensively using the Taylor diagram.

Materials

Dataset description

In recent years, artificial intelligence approaches have been widely utilized in engineering problems (Esmaeili-Falak 2017, Esmaeili-Falak *et al.* 2019, Benemaran and Esmaeili-Falak 2020). This study aims to evaluate the application of XGB-based approaches for predicting the M_R of subbase materials and subgrade soils. The dataset utilized for developing the XGB models to predict the M_R of the flexible pavement foundation were collected from a total of 891 records reported in former studies carried out by other researchers (Kim 1999, 2004, Huang 2001, Rodgers 2006) on various types of soils classified as A-1 (A-1-a, A-1-b), A-2 (A-2-4), A-4, A-6 and A-7 (A-7-6), according to AASHTO soil classification system that which approximately cover all type of the soils from gravel to clay. However, it should be mentioned that the present study and the developed models are site-specific, and the results should be employed conservatively in practical projects. The dataset contains some physical and mechanical properties of soil like the type of soil, P#200, PI, LL, S_r, q_u, ω_{opt}, ω_c, σ_o, and σ_d, where:

- ***P*#200:** Percent passing through the No. 200 sieve is an important index that represents the materials' clay and silt content. There are direct relationships between the expansion of elastic and plastic deformations with the percentage of clay and silt under traffic loading.

- ***PI* and *LL*:** The PI, Plasticity Index is the difference between the liquid limit and the plastic limit, while the LL is defined as the lowest moisture content of soil at which it flows like a liquid. The plasticity index and liquid limit are indicators that provide the connection between pore water and sub-base.
- **σ_o, and σ_d**: The confining pressure and deviatoric stress are independent parameters for materials' strength based on Mohr-Coulomb theory.
- **S_r, ω_{opt}, and ω_c:** The degree of saturation, optimum water content, and natural water content has an important effect on soils' strength. If the soil's natural water content ω_c is different of the ω_{opt}, soil strength will be varied.
- **q_u**: The soils' M_R may increase with increasing unconfined compressive strength (q_u).

By incorporating most of the influential parameters and using the existing database, a model is developed to predict the resilient modulus of cohesive subgrade soils as a function of the following parameters:

$$M_R = f(P\#200, PI, LL, \sigma_o, \sigma_d,\ S_r, \omega_{opt}, \omega_c, and\ \ q_u) \quad (1)$$

The violin plots are indicated in Fig. 1, where present dependent and independent distribution, along with the analysis of outliers. Also, the relationship between two parameters can be calculated using the Pearson correlation coefficient (PCC) as:

$$\rho_{X,Y} = \frac{cov(X,Y)}{\sigma_X \sigma_Y} \quad (2)$$

where $cov(X,Y)$ is the covariance between X and Y and σ_X and σ_Y are the standard deviations of X and Y. The PCC between considered variables has been visualized by a correlation matrix as presented in Fig. 2. The high value of positive or

negative coefficients could affect the model's accuracy and the difficulty in interpreting the effects of the input parameters on the target parameter. It could be seen that PCC between q_u, σ_o, and σ_d with other variables is very small, indicating that these variables parameters shall not causes multicollinearity problems on models (Farrar and Glauber 1967). Also, the PCC between M_R and other variables is fairly small, except with S_r (-0.6007). Furthermore, the correlations between LL and PI, LL and ω_{opt}, and ω_c with ω_{opt} are extremely high. Finally, there is moderate correlation between $P\#200$ and LL, PI, ω_c and ω_{opt}.

Artificial intelligence-based methods use data to develop an optimal model, where the best relationship between input and output parameters is achieved. One of the main problems that should be avoided when finding the best model is known as overfitting. This problem is encountered when the developed model has a small error but resultsin an extremely large error when used with a different dataset. To elude overfitting, the dataset should be divided into two subsets, namely training data and testing data. The training dataset is utilized to build the model, and then the predictive capabilities of the trained model are examined on the unused testing data. Several studies recommended using 20 to 30% of the data to test the performance of the trained model (Shahin *et al.* 2004, Saptoro *et al.* 2012, Gandomi *et al.* 2013, Ghorbani *et al.* 2020, Heidarabadizadeh *et al.* 2021, Kayadelen *et al.* 2021). In the present study, 75% and 25% of the dataset were employed for the training and testing phases, respectively. Table 2 presents some statistical indices of the input parameters. Also, Fig. 3 depicts the histogram of variables and their normal distribution plots for the training and testing data.

The dataset's 3D surface plots resulting from interpolation with a thin-plate spline are presented in Fig. 4. The soil properties indicate complex and remarkably

nonlinear relationships between input variables and output. For example, in Fig. 4a, M_R tends to be high for significant q_u values (roughly 700 kPa) and with a peak region of M_R for P#200 at about 100%. As another example, Fig. 4d depicts the relationship between σ_o and σ_d with M_R, where for σ_d values of around 0 kPa and σ_o of about 30 kPa, M_R has the highest value of about 150 MPa. Similar tendencies are detected in other plots suggesting a specific range or domain where the M_R is maximum.

Fig. 5 shows the overall analysis process of the XGB models developed in this article. According to this flowchart, the analysis procedure is divided into five stages: (1) dataset collection; (2) dataset interpretation; (3) model creation; (4) model verification and evaluation; (5) outcome assessment. Four integrated XGB designs are developed to predicting M_R using different optimization algorithms ($SCA-XGB$, $PSO-XGB$, $SSO-XGB$, and $MVO-XGB$). The models were coded in MATLAB 2018b on a PC with Intel (R) Core (TM) i7-8750H CPU @ 2.20GHz microprocessor with RAM of 16 GB.

Methodological overview

Extreme gradient boosting (XGB) method

The XGB's base is the hybrid algorithm by gradient boosting tree (Chen *et al.* 2015). Gradient boosting is a representative algorithm for enhancing the ensemble algorithm. XGB algorithm is a powerful performance type of the gradient boosting method. Excessive GB is identical to gradient boosting tree, that is based on the retrogression and categorization tree (Le *et al.* 2019, Yang *et al.* 2019, Zhou, Li, Wang, *et al.* 2019, Zhou, Li, Yang, *et al.* 2019, Ding *et al.* 2020, Zhang *et al.* 2021). It can create feeble multiplex evaluations on the data collection via summarizing the modeling outcomes of

the feeble evaluations. Simultaneously, the XGB method can effectually perform with categorization and regression problems to gain higher output than a seperate one (Yang *et al.* 2019, Zhou, Li, Wang, *et al.* 2019). Practically, it can be symbolized as a smooth calculating library that merges a novel algorithm with the gradient boosting intention tree approach.

The objective function of hybrid XGB reduces conditions that control it to prevent over-fitting (Chen and Guestrin 2016), then the objective function is produced with several parts. The initial part is used to compute the differences between the predicted amount and the measured value, and the final part is the regularization point. The predicting accuracy of the algorithm is determined by the deflection and variant of the algorithm. $D = \{(xi, yi)\}$ is a class of data including m attributes, n specimens, and the predictor is a surplus system created of k basis systems. Specimen forecasting results can be presented as:

$$\hat{y}_i = \sum_{k=1}^{K} f_k(x_i), f_k \in \varphi \tag{3}$$

$$\varphi = \{f(x) = w_s(x)\}(s: R^m \to T, w_s \in R^T) \tag{4}$$

x_i : One of the samples

$f_k(x_i)$: Estimation points for a specific specimen

φ : The collection of regression trees

s : Structural variable

w : The weight of the Leaf

T : The leaves' number

K : The trees' number

$\hat{y}_i$: The predicted label

To procure the least dissipation and optimize the ensemble tree, XGB shows the model difficulty to compute the procedure performance of the algorithm. Accordingly, the objective efficiency consists of the usual dissipation efficiency and the model difficulty.

$$Obj^{(t)} = \sum_{i=1}^{m} l\left(y_i^t, \hat{y}_i^{(t-1)} + f_t(x_i)\right) + \sum_{k=1}^{t} \Omega(f_k) \tag{5}$$

$$\Omega(f_k) = \gamma T + \frac{1}{2}\lambda \|w\|^2 \tag{6}$$

Here, i and m are the numbers of specimens in the database and the total number of records brought in the k^{th} tree. The first term in Eq. (5) presents the usual dissipation function, computing the discrepancy between the predicted and measured values. The second term in Eq. (5) presents the difficulty of the algorithm. Moreover, γ and λ are variables which could redact the difficulty of the tree, as well as the arrangement point assists in keeping far from over-compatibility by adjusting the final weights.

Then, for better simplification of the objective term, Taylor's explanation is performed:

$$Obj^{(t)} = \sum_{i=1}^{m} \left[f_t(x_i) g_i + \frac{1}{2}\left(f_t(x_i)\right)^2 h_i\right] + \gamma T + 0.5\lambda \sum_{j=1}^{T} w_j^2 \tag{7}$$

where g_i and h_i show the first and second derivatives gained on the loss function, respectively.

Sine–cosine algorithm (SCA)

After generating a random set of solutions, the SCA method is a population technique for finding the best possible answer. In the duration of computing, the possibility of obtaining wonderful answers increases, and the most proper answer is obtained after

receiving sufficient solutions. The exploration and exploitation stages of this algorithm's computing technique are split into two major phases, and the position of the solution is updated according to the given rule. (Mirjalili 2016):

$$X_i^{t+1} = \begin{cases} X_i^t + r_1 \times \sin r_2 \times |r_3 P_i^t - X_i^t| & r_4 < 0.5 \\ X_i^t + r_1 \times \cos r_2 \times |r_3 P_i^t - X_i^t| & r_4 \geq 0.5 \end{cases} \quad (8)$$

where X^{t+1} shows the solution's position in the i^{th} dimension and t^{th} iteration, and P^t shows the target goal spot in the i^{th} dimension. Furthermore, $r_1 - r_4$ indicate random values.

The spread of the sine and cosine is compatibly modified based on this optimization strategy to balance the exploration and exploitation stages (Fig. 6) using the following formula. (Mirjalili 2016):

$$r_1 = a - t\frac{a}{T} \quad (9)$$

where t shows the iterations' maximum number, T shows the present iteration, and a stands for a constant.

Multi-verse optimization algorithm (MVO)

MVO is one of the recent optimization algorithms infused by nature (Fig. 7). The original revelation of this algorithm was obtained from the theory of multi-verse in astrophysics. In the present state, multiple big bangs from multiple cosmoses interrelate together through white, black, and wormholes (Mirjalili *et al.* 2016). It was mentioned in the base article of MVO that matters transport between two cosmoses through a conduit with a black and white hole. White ones throw out the matters, and dark ones absorb. A worm one develops a conduit through time and joins other sections of the cosmos with each other. It is worth mentioning that the available phrases are utilized in the entire part when proposing the MVO algorithm: a cosmos shows an answer, a thing

communicates, time demonstrates a descendent, and swell rate depicts the objective amount of a galaxy.

In MVO, each solution is known as a cosmos with an opportunity to include white, black, warm holes. To enhance the modality of each solution, it's considered that substance emitters are presumably to combine in a solution with a bigger objective amount. Matter attractors are expected to be developed in a solution with an inferior than that of the objective amount. With this process, variables' amounts from good answers are transported to a bad solution. The main mathematical algorithm of MVO appertains in Eqs. (10-11):

$$X_i^j = \begin{Bmatrix} X_k^j, & r_1 < NI(U_i) \\ X_i^j, & r_1 \geq NI(U_i) \end{Bmatrix} \tag{10}$$

X_i^j : The j_{th} thing of the i_{th} universe

r_1 : An accidental number between 0-1

$NI(U_i)$: The normalized swell rate of the i_{th} universe

X_k^j The j_{th} thing of the k_{th} universe

$$X_i^j = \begin{Bmatrix} \begin{Bmatrix} (X_j + TDR \times (ub - lb) \times r_4 + lb), & r_3 < 0.5 \\ (X_j - TDR \times (ub - lb) \times r_4 + lb), & r_3 \geq 0.5 \end{Bmatrix}, & r_2 < WEP \\ X_i^j, & r_2 \geq WEP \end{Bmatrix} \tag{11}$$

X_j : The j_{th} centroid of the best universe obtained up to now

u_b : The largest point

l_b : The lowest point

r_2, r_3, r_4 : Random numbers between 0-1.

where traveling distance rate (TDR) and Wormhole Existence Probability (WEP) are coefficients.

Moreover, the MVO algorithm holds the main solution during optimization and applies it to strike the residual solutions. It was shown that exists wormholes nominated between the main answer and other ones, and the varier can be interchanged easily. Again, these ascent the feasibility of improving the solution and holding the main solution obtained until now during the optimizing process. The main answer went back to the final optimal as the main calculation of the general optimal for the observed problem.

The mentioned relations and subordinates require MVO for parameters exchanging between answers. Thus, they result in identical exploitation and exploration type if it's utilized with a non-Adaptive process. The process is employed in the MVO to suitably verify discovery and operation in several phases of optimizing procedure.

$$WEP = min + l \times (\frac{max - min}{L}) \tag{12}$$

$$TDR = 1 - \frac{l^{1/p}}{L^{1/p}} \tag{13}$$

where min is minimum with a generic amount of 0.2, max is maximum with a generic amount of 1, l is the running repetition, L shows the maximum iterations and p defines the operation factor.

MVO has two robust variables: WEP and TDR. WEP raises proportionally to the numeral of repetition to increment operation. TDR is raised up to the iteration to obtain a very accurate operation/local search over the main solution gained.

This optimization method is a solstitial algorithm until the universe exchanges matters. This communicates to intersecting term, that is a generic solstitial function. This leads to abrupt variations in the resulting cosmos, enhances figuring out of the searching prospect, and sustain the differences of cosmoses in repetitions.

Also, each cosmos picks some variables randomly from the main answers. This communicates exchange, which is a famed solstitial function in the solstitial algorithm. The conversion factor is the cause of small changes in an answer and enhances operation. Another solstitial term is called elitism, which holds the main answer received up to now in the optimization. This term is ended by collecting the main cosmos created up to the moment.

Consider that the computational difficulty of the MVO is of $O(tnd)$ where t demonstrates the highest quantity of posterities, n presents the quantity of cosmoses, and d describes the number of variables. Since the consequence of the objective operation pertains to the problem, it has not been included in the algorithm difficulty. Suppose the difficulty of the objective operator is known. In that case, it is good to be multiplied using n and t since the objective value is calculated for each universe in each iteration. Here, difficulty can be shown as $(tn(cof + d))$, where cof is subordinate to the cost of the target.

Particle swarm optimization (PSO)

PSO recognized as a computational method which optimizes a particular issue utilizing frequent rectifying nominate solutions, here called particles (Kennedy and Eberhart 1995). Every location vector of a particle is presented by X_i^k, speed vector by V_i^k , and fitness value, where i and k are the available production and the i_{th} particle. During the exploration area, referred particles go forward to global premier locations based on the premier position and local speed. Here, the smallest value of fitness determines the proper position (Xue 2018). Eqs. (14-15) update the speed of every particle.

$$V_i^{k+1} = \omega V_i^k + c_1 r_1 P_i^k - X_i^k + c_2 r_2 P_g^k - X_i^k \tag{14}$$

$$X_i^{k+1} = X_i^k + V_i^{k+1} \tag{15}$$

c_1 and c_2 : Coefficients of Acceleration

ω : Inertia weight $(= 1)$

r_1 and r_2 : Accidental numbers $[0, 1]$

P_i : The present most proper position of i_{th} particles

P_g : The best global

The lowest and highest value of V_i^k are -1 and 1, respectively. In this method, parameters of $\omega,\ c_1\ and\ c_2$ need to be modified, as their values impact the isotopy speed. For that, to raise this optimization efficiency by variable parameters, a different instance of choosing PSO parameters can be found in the literature (Shi and Eberhart 1998, Trelea 2003, Khoshaim *et al.* 2021).

Social Spider Optimization (SSO)

SSO has been developed based on the collaborative treatment of social spiders. Both genders female and male find spiders are observed by the optimization method (Cuevas *et al.* 2013). The social spider association includes two main sections: its association network and its organs. Based on the various spiders' genders, all organs are apportioned to two different groups, and every factor is managed by a group of various operators to imitate the collaborative treatment in the group. Between them, the male gender's populaces are to apportioned into influential and uninfluential classes. Influential group spiders have superior compatibility than uninfluential group spiders. In the general web, they are possessed by the nearest female kind of spider. On the other side, the uninfluential male spiders are inclined to be focused in the middle of the male populace for the use of the sources dissipated by influential male spiders. Every spider will carry the heaviness based on the fitness value of the solution represented by the social spider:

$$w_t = \frac{fitness_t - Worst}{Best - Worst} \tag{16}$$

where fitness$_{(t)}$ shows the suitability value gained by appraising the location of t^{th} spider, $t = 1, 2, \dots, T$. Best represents the best value, and worst represents the worst value of the whole populace.

SSO assumes that the whole exploration area is a general web where all social spiders interrelate with others. Every solution in the exploration area shows the spider's position in the general network. (Fig. 8).

Models' assessment metrics

The justification and assessment of the developed models is the main stage. After building the models, it is necessary to recognize that they have enough precise results for the prediction and simulation aims. The efficiency of the training and testing data has been used to assess the accuracy of the above-mentioned approaches. In the present paper, six statistical criteria were used to evaluate the model performance and its accuracy. These include the coefficient of determination (R^2), root mean square error ($RMSE$), mean absolute error (MAE), the variance accounted factor (VAF), performance index (PI), and $A_{10-index}$. The smaller $RMSE$ and MAE and larger VAF show more trustable statistical impressions. The larger R^2 depicts a better correlation between the observed and simulated output. It is worth explaining that a new evaluator ($A_{10-index}$) also analyzed, where $A_{10-index}$ equal to 1.0 depicts a wonderful estimating model.

$$R^2 = \left(\frac{\sum_{p=1}^{P}(t_P - \bar{t})(y_P - \bar{y})}{\sqrt{\left[\sum_{p=1}^{P}(t_P - \bar{t})^2\right]\left[\sum_{p=1}^{P}(y_P - \bar{y})^2\right]}} \right)^2 \tag{17}$$

$$RMSE = \sqrt{\frac{1}{P}\sum_{p=1}^{P}\left(y_p - t_p\right)^2} \quad (18)$$

$$MAE = \frac{1}{P}\sum_{p=1}^{P}\left|y_p - t_p\right| \quad (19)$$

$$VAF = \left(1 - \frac{var(t_P - y_P)}{var(t_P)}\right) * 100 \quad (20)$$

$$PI = \frac{1}{|\bar{t}|}\frac{RMSE}{\sqrt{R^2} + 1} \quad (21)$$

$$A_{10-index} = \frac{m_{10}}{M} \quad (22)$$

where y_P and t_P are the simulated and observed values, and $\bar{t}$ and $\bar{y}$ are the mean of the observed and simulated values, respectively. As well, M represents the sample number, and m_{10} is the number of records with a ratio of measured to predicted value between 0.9 and 1.1.

Result and discussion

The XGB-based models were developed using the procedure described in Fig. 5. First, the input variables of the XGB models were identified, and the database was prepared. The corresponding variables for each optimization algorithm were then calibrated, as shown in Table 3. The optimization procedure resulted in the optimized parameters of the hybrid models, which are also presented in Table 3.

For the employed $PSO - XGB$, $SCA - XGB$, $MVO - XGB$, and $SSO - XGB$ hybrid models, the $RMSE$-based convergence diagram of the proposed functions is shown in Fig. 9. It can be seen from the figure that the $SSO - XGB$ model rapidly converged and attained the lowermost value of $RMSE$ at the least number of iterations

in comparison with other hybrid models. The $SSO - XGB$ model achieved $RMSE$ (fitness) value of 3.1915 in 32 iterations; these values for $SCA - XGB$ and $MVO - XGB$ models were 3.8449 in 102 iterations and 3.48161 in 61 iterations, respectively. The fitness value of $PSO - XGB$ was almost the same as $MVO - XGB$ but at a slightly lesser number of iterations.

Four performance evaluation indices, R^2, $RMSE$, MAE, and $A_{10-index}$, were determined for the above-mentioned models, and the results are presented in Fig. 10a, 10b for the training and testing data, respectively. As shown in Fig. 10a, based on R^2 and $RMSE$, the $SSO - XGB$ model has the best accuracy; while considering total scores obtained from the training and testing section by summing the scores of all indices, the $SCA - XGB$ model has the lowest accuracy. From Fig. 10b, based on $RMSE$ and MAE, $PSO - XGB$ is the most accurate predictive model; however, when considering R^2 and A_{10}-index, $SCA - XGB$, and $PSO - XGB$ have the best precision, respectively. $SSO - XGB$ has the lowest accuracy considering all four performance evaluation indices.

It can be seen that the four optimization algorithms are intended to detect the optimized parameters of XGB-based models. Six model performance indices (R^2, $RMSE$, MAE, PI, VAF, and $A_{10-index}$) were assessed to have the best comparison. The models were scored from 1 to 4 based on each of the six indices; then, the scores were summed to assign a total score for each model. Results for this comparisonare gathered in Table 4.

The results demonstrated that all techniques have an acceptable efficiency in forecasting the resilient modulus of flexible pavement foundation, illustrating a reasonable relationship between measured and estimated values and models' robustness. Evaluating the results listed in Table 4 shows that both $SSO - XGB$ and $PSO - XGB$ have the best performance considering the training data, while for testing data $PSO -$

XGB has the highest accuracy. On the other hand, $SCA-XGB$ and $SSO-XGB$ models have the lowest accuracy for training and testing data, respectively.

Fig. 11 illustrates the efficiency of each optimized technique, which shows the total ranking in the form of an intuitive stacked diagram. All in all, considering both training and testing data, $PSO-XGB$, $MVO-XGB$, $SSO-XGB$, and $SCA-XGB$ models have the highest to lowest accuracy.

Fig. 12 presents the relationship between the predicted and measured values for the training and testing data. The results for the training data show that the models have been able to capture and learn the relationship between M_R and the contributing input parameters with very good accuracy. Considering R^2, $RMSE$, PI, and VAF indices, the $SSO-XGB$ model has better for the training data with corresponding amounts of 0.9918, 2.7047, 0.025, and 99.1774, respectively. The training results of the $SCA-XGB$ hybrid model show the lowest accuracy from the viewpoint of R^2, $RMSE$, MAE, PI, and VAF indices, equal to 0.9895, 3.2041, 2.2765 0.0296, and 98.942, respectively. The R^2 values of the above-mentioned models are more than 0.989, representing an excellent match for the training results.

After completing the model training, the testing database was used to validate and assess the performance of these four optimized XGB-based models in predicting unseen cases. As shown in Fig. 12, by evaluating the correlation between the predicted and actual values of M_R, it is obvious that the testing data points are almost scattered along the 45-degree line (predicted M_R=Measured M_R), similar to the case of the training data set. This shows that the testing results of developed models are also outstanding. Considering the $RMSE$, MAE, PI, and $A_{10-index}$ (which are equal to 4.8442, 3.2966, 0.0432, and 0.7803 respectively), the $PSO-XGB$ hybrid model has the

highest accuracy for the testing results. Considering all six performance evaluation criteria, the $SSO-XGB$ hybrid technique has the lowest prediction accuracy.

Figs. 13-16 show that the predicted results of the $PSO-XGB$, $MVO-XGB$, $SCA-XGB$, and $SSO-XGB$ models, along with the corresponding measured values, as well as the prediction errors and error distribution for both training and testing datasets. Figs. 13a-16a demonstrate the scatter diagrams of the measured values of M_R along with the predicted ones, showing an excellent correlation between the measured and estimated results. Figs. 10-13 (b, c) show that most distribution of errors occurs around the zero point, which leads to a great accuracy of the models. All the developed models lead to more spot distribution around zero points in the form of a Gaussian bell.

The Taylor diagram of the developed models of M_R of the flexible pavement foundation is presented in Fig. 17. It is seen from these graphs that, despite the excellent performance of all models in high-precision estimation of the M_R, $SSO-XGB$ and $PSO-XGB$ hybrid models have the best performance in predicting both training and testing data, while the $SCA-XGB$ hybrid model has the worst performance in predicting both training and testing data. The $PSO-XGB$ model also has a good performance in predicting the M_R of flexible pavement foundation considering both the training and testing data.

According to the literature, in order to develop a resilient modulus of flexible pavement foundations, several variables can be chosen as inputs, such as P#200, PI, LL, σ_o, σ_d, $S_r, \omega_{opt}, \omega_c$, q_u, γ_d, C_u, and θ. Different studies have used various combinations of these inputs to develop models. The main purpose of these types of studies is to propose the model with the highest accuracy. Also, as more variables utilize as inputs, vast attributes of the problem would be involved in the model and increase the model's comprehensiveness. Table 5 presents the related works on this

topic. Between all developed models in the literature, the suggested $PSO-XGB$ model from this study outperforms all models by introducing various inputs (P#200, PI, LL, $\sigma_o, \sigma_d,\ S_r, \omega_{opt}, \omega_c,\ and\ \ q_u$), at R^2 equal to 0.9911 and RMSE equal to 2.9306. Just one model ($SVM-CBO$) had a proper performance with R^2 value of 0.9978 (Heidarabadizadeh et al. 2021). However, herein, the value of $RMSE$ for $SVM-CBO$ was lower than $PSO-XGB$, and this study introduced higher number of input variables leads to raise model's generalization respect to $SVM-CBO$ (γ_d, C_u, P#200, PI, $\sigma_o, \sigma_d, and\ \omega_{opt}$).

Sensitivity analysis

The performance of the developed models was evaluated through a sensitivity analysis to identify the parameters with high, moderate, and low importance. The $PSO-XGB$ model was selected to perform the sensitivity analysis due to its highly accurate performance. Table 6 shows the effect of removing each parameter on the values of R^2 and $RMSE$ indices for the testing data. As shown in this table, the developed hybrid $PSO-XGB$ model demonstrates the highest sensitivity to the "confining pressure" parameter considering both R^2 and $RMSE$ indices.

For the R^2 index, elimination of $P\#200$, LL, PI, σ_0, σ_d, S_r, ω_{opt}, ω_c and q_u parameters lead to -0.16%, -0.22%, 0.23%, -25.03%, -6.78%, -1.12%, -0.06%, -0.05% and 0.16% variation in the testing data, respectively, while considering the $RMSE$ index, these values increase +0.1769, +0.1719, -0.1786, +10.3366, +4.0665, +0.8618, +0.1434, +0.1254 and + 0.2928 units, respectively. Considering $RMSE$, eliminating both the confining pressure and deviatoric stress has a relatively high effect on the predicted M_R, and the effect of other parameters is almost similar.

Conclusions

In this study, various meta-heuristic algorithms (PSO, SCA, MVO, and SSO) were used to enhance the prediction accuracy of the XGB-based approach in estimating the resilient modulus of flexible pavement foundations. The vital parameters of the XGB-based models were optimized, leading to hybrid $PSO-XGB$, $SCA-XGB$, $MVO-XGB$, and $SSO-XGB$ approaches. An extensive database was prepared from the technical literature and used to develop models to predict the resilient modulus of the flexible pavement foundations as a function of percent passing through No. 200 sieve, plasticity index, liquid limit, confining pressure, deviatoric stress, degree of saturation, optimum water content, natural water content and unconfined compressive strength. The main conclusions drawn from this study are as follows:

- All of the models developed in this study have a good performance in predicting the M_R of flexible pavement foundation, as the predicted values are in good agreement with the actual values.
- Six model performance evaluation indices, R^2, $RMSE$, MAE, VAF, PI, and $A_{10-index}$, were employed to assess the performance of the developed models. It was shown that all hybrid XGB-based models have reasonable accuracy in predicting the M_R.
- Considering the training data, $SSO-XGB$ and $PSO-XGB$ models have the best performance, while the $PSO-XGB$ model has high accuracy predictions for the testing data. Overall, $PSO-XGB$ is presented as the best hybrid model for predicting the M_R of flexible pavement foundation.
- The Taylor diagram showed that despite the excellent performance of all techniques in accurate prediction of the M_R, $SSO-XGB$, and $PSO-XGB$ hybrid models have the best performance in predicting both training and testing.

- The results of the sensitivity analysis showed that the developed hybrid $PSO-XGB$ model has the highest sensitivity to the "confining pressure" parameter considering both R^2 and RMSE indices.

References:

AASHTO, T., 2003. 307, Determining the Resilient Modulus of Soils and Aggregate Materials, Standard Specifications for Transportation Materials and Methods of Sampling and Testing, Washington, D.

Asphalt Institute, 1982. *Research and Development of the Asphalt Institute's Thickness Design Manual*. Asphalt Institute.

Bardhan, A., Gokceoglu, C., Burman, A., Samui, P., and Asteris, P.G., 2021. Efficient computational techniques for predicting the California bearing ratio of soil in soaked conditions. *Engineering Geology*, 106239.

Barksdale, R.D., Lago Alba, J.A., Khosla, N.P., Kim, R., Lambe, P.C., and Rahman, M.S., 1997. *Laboratory determination of resilient modulus for flexible pavement design*.

Benemaran, R.S. and Esmaeili-Falak, M., 2020. Optimization of cost and mechanical properties of concrete with admixtures using MARS and PSO. *Computers and Concrete*, 26 (4), 309–316.

Chen, T. and Guestrin, C., 2016. XGBoost. *In*: *Proceedings of the 22nd ACM SIGKDD International Conference on Knowledge Discovery and Data Mining*. New York, NY, USA: ACM, 785–794.

Chen, T., He, T., Benesty, M., Khotilovich, V., Tang, Y., and Cho, H., 2015. Xgboost: extreme gradient boosting. *R package version 0.4-2*, 1 (4), 1–4.

Chou, J.-S., Chong, W.K., and Bui, D.-K., 2016. Nature-inspired metaheuristic

regression system: programming and implementation for civil engineering applications. *Journal of Computing in Civil Engineering*, 30 (5), 4016007.

Corrêa-Silva, M., Rouainia, M., Miranda, T., and Cristelo, N., 2021. Predicting the mechanical behaviour of a sandy clay stabilised with an alkali-activated binder. *Engineering Geology*, 292, 106260.

Cuevas, E., Cienfuegos, M., Zaldívar, D., and Pérez-Cisneros, M., 2013. A swarm optimization algorithm inspired in the behavior of the social-spider. *Expert Systems with Applications*, 40 (16), 6374–6384.

Ding, Z., Nguyen, H., Bui, X.-N., Zhou, J., and Moayedi, H., 2020. Computational intelligence model for estimating intensity of blast-induced ground vibration in a mine based on imperialist competitive and extreme gradient boosting algorithms. *Natural Resources Research*, 29 (2), 751–769.

Dunlap, W.A., 1963. *A report on a mathematical model describing the deformation characteristics of granular materials*. Texas Transportation Institute, Texas A & M University.

Ebrahimi, A., 2006. Regression and neural network modeling of resilient modulus based on routine soil properties and stress states.

Esmaeili-Falak, M., 2017. Effect of system's geometry on the stability of frozen wall in excavation of saturated granular soils. Doctoral dissertation, University of Tabriz.

Esmaeili-Falak, M., Katebi, H., and Javadi, A., 2018. Experimental study of the mechanical behavior of frozen soils-A case study of tabriz subway. *Periodica Polytechnica Civil Engineering*, 62 (1), 117–125.

Esmaeili-Falak, M., Katebi, H., Javadi, A., and Rahimi, S., 2017. Experimental investigation of stress and strain characteristics of frozen sandy soils-A case study of Tabriz subway. *Modares Civil Engineering journal*, 17 (5), 13–23.

Esmaeili-Falak, M., Katebi, H., and Javadi, A.A., 2020. Effect of Freezing on Stress–Strain Characteristics of Granular and Cohesive Soils. *Journal of Cold Regions Engineering*, 34 (2), 5020001.

Esmaeili-Falak, M., Katebi, H., Vadiati, M., and Adamowski, J., 2019. Predicting triaxial compressive strength and Young's modulus of frozen sand using artificial intelligence methods. *Journal of Cold Regions Engineering*, 33 (3), 4019007.

Farrar, D.E. and Glauber, R.R., 1967. Multicollinearity in regression analysis: the problem revisited. *The Review of Economic and Statistics*, 92–107.

Feng, Z., Niu, W., Liu, S., Luo, B., Miao, S., and Liu, K., 2020. Multiple hydropower reservoirs operation optimization by adaptive mutation sine cosine algorithm based on neighborhood search and simplex search strategies. *Journal of Hydrology*, 590, 125223.

de Freitas, J.B., de Rezende, L.R., and de FN Gitirana Jr, G., 2020. Prediction of the resilient modulus of two tropical subgrade soils considering unsaturated conditions. *Engineering Geology*, 270, 105580.

Gandomi, A.H., Yang, X.-S., Talatahari, S., and Alavi, A.H., 2013. Metaheuristic algorithms in modeling and optimization. *Metaheuristic applications in structures and infrastructures*, 1–24.

Ghanizadeh, A.R. and Tavana Amlashi, A., 2018. Prediction of fine-grained soils resilient modulus using hybrid ANN-PSO, SVM-PSO and ANFIS-PSO methods. *Quarterly Journal of Transportation Engineering*, 9 (special), 159–181.

Ghorbani, B., Arulrajah, A., Narsilio, G., Horpibulsuk, S., and Bo, M.W., 2020. Development of genetic-based models for predicting the resilient modulus of cohesive pavement subgrade soils. *Soils and Foundations*, 60 (2), 398–412.

Han, G., Zhang, C., Zhou, H., Zhang, C., Gao, Y., and Singh, H.K., 2021. A new

predictive method for the shear strength of interlayer shear weakness zone at field scales. *Engineering Geology*, 106449.

Han, Z. and Vanapalli, S.K., 2016. Relationship between resilient modulus and suction for compacted subgrade soils. *Engineering Geology*, 211, 85–97.

Hanittinan, W., 2007. Resilient modulus prediction using neural network algorithm.

Heidarabadizadeh, N., Ghanizadeh, A.R., and Behnood, A., 2021. Prediction of the resilient modulus of non-cohesive subgrade soils and unbound subbase materials using a hybrid support vector machine method and colliding bodies optimization algorithm. *Construction and Building Materials*, 275, 122140.

Heukelom, W. and Klomp, A., 1962. Dynamic testing as a means of controlling pavements during and after construction. *In*: *International Conference on the Structural Design of Asphalt PavementsUniversity of Michigan, Ann Arbor*.

Huang, J., 2001. Degradation of resilient modulus of saturated clay due to pore water pressure buildup under cyclic loading.

Huang, Y.H., 1993. *Pavement analysis and design*.

Kayadelen, C., Altay, G., and Önal, Y., 2021. Numerical simulation and novel methodology on resilient modulus for traffic loading on road embankment. *International Journal of Pavement Engineering*, 1–10.

Kennedy, J. and Eberhart, R., 1995. Particle swarm optimization. *In*: *Proceedings of ICNN'95-international conference on neural networks*. IEEE, 1942–1948.

Khasawneh, M.A., 2005. Laboratory characterization of cohesive subgrade materials.

Khoshaim, A.B., Elsheikh, A.H., Moustafa, E.B., Basha, M., and Mosleh, A.O., 2021. Prediction of residual stresses in turning of pure iron using artificial intelligence-based methods. *Journal of Materials Research and Technology*, 11, 2181–2194.

Kim, D.-G., 1999. Engineering properties affecting the resilient modulus of fine-grained

soils as subgrade.

Kim, D.-G., 2004. *Development of a constitutive model for resilient modulus of cohesive soils*. The Ohio State University.

Kumar, P., Dilip, D.M., and Babu, G.L., 2014. Critical appraisal of correlations between CBR and subgrade modulus. *In*: *Journal of the Indian Roads Congress*.

Le, L.T., Nguyen, H., Zhou, J., Dou, J., and Moayedi, H., 2019. Estimating the heating load of buildings for smart city planning using a novel artificial intelligence technique PSO-XGBoost. *Applied Sciences*, 9 (13), 2714.

Lee, D.-H., Cheon, E., Lim, H.-H., Choi, S.-K., Kim, Y.-T., and Lee, S.-R., 2021. An artificial neural network model to predict debris-flow volumes caused by extreme rainfall in the central region of South Korea. *Engineering Geology*, 281, 105979.

Lei, H., Zhang, W., Wang, L., Feng, S., Song, Y., and Qi, Z., 2021. An empirical model for predicting pore pressure development in artificial freeze-thaw soft clay under cyclic loading. *Engineering Geology*, 106425.

Liu, L., He, H., Dyck, M., and Lv, J., 2021. Modeling thermal conductivity of clays: A review and evaluation of 28 predictive models. *Engineering Geology*, 106107.

Liu, S., Zou, H., Cai, G., Bheemasetti, T.V., Puppala, A.J., and Lin, J., 2016. Multivariate correlation among resilient modulus and cone penetration test parameters of cohesive subgrade soils. *Engineering Geology*, 209, 128–142.

Mirjalili, S., 2016. SCA: a sine cosine algorithm for solving optimization problems. *Knowledge-based systems*, 96, 120–133.

Mirjalili, S., Mirjalili, S.M., and Hatamlou, A., 2016. Multi-verse optimizer: a nature-inspired algorithm for global optimization. *Neural Computing and Applications*, 27 (2), 495–513.

Moossazadeh, J. and Witczak, M.W., 1981. Prediction of subgrade moduli for soil that

exhibits nonlinear behavior. *Transportation Research Record*, (810).

Nazzal, M.D. and Mohammad, L.N., 2010. Estimation of resilient modulus of subgrade soils for design of pavement structures. *Journal of Materials in Civil Engineering*, 22 (7), 726–734.

Nazzal, M.D. and Tatari, O., 2013. Evaluating the use of neural networks and genetic algorithms for prediction of subgrade resilient modulus. *International Journal of Pavement Engineering*, 14 (4), 364–373.

Ni, B., Hopkins, T.C., Sun, L., and Beckham, T.L., 2020. Modeling the resilient modulus of soils. *In*: *Bearing Capacity of Roads, Railways and Airfields*. CRC Press, 1131–1142.

Ozsahin, T.S. and Oruc, S., 2008. Neural network model for resilient modulus of emulsified asphalt mixtures. *Construction and Building Materials*, 22 (7), 1436–1445.

Pal, M. and Deswal, S., 2014. Extreme learning machine based modeling of resilient modulus of subgrade soils. *Geotechnical and Geological Engineering*, 32 (2), 287–296.

Park, H.I., Kweon, G.C., and Lee, S.R., 2009. Prediction of resilient modulus of granular subgrade soils and subbase materials using artificial neural network. *Road Materials and Pavement Design*, 10 (3), 647–665.

PDG, M.E., 2004. NCHRP-Guide for mechanistic-empirical design of new and rehabilitated pavement structures. National Cooperative Highway Research Program. *Transportation Research Board, National Research Council, Washington, DC, USA*.

Poorjafar, A., Esmaeili-Falak, M., and Katebi, H., 2021. Pile-soil interaction determined by laterally loaded fixed head pile group. *Geomechanics and Engineering*, 26 (1),

13–25.

Pourtahmasb, M.S., Karim, M.R., and Shamshirband, S., 2015. Resilient modulus prediction of asphalt mixtures containing recycled concrete aggregate using an adaptive neuro-fuzzy methodology. *Construction and Building Materials*, 82, 257–263.

Rahim, A.M., 2005. Subgrade soil index properties to estimate resilient modulus for pavement design. *International Journal of Pavement Engineering*, 6 (3), 163–169.

Rodgers, G.A., 2006. Resilient modulus predictions using engineering properties and neural networks.

Sadrossadat, E., Heidaripanah, A., and Ghorbani, B., 2018. Towards application of linear genetic programming for indirect estimation of the resilient modulus of pavements subgrade soils. *Road Materials and Pavement Design*, 19 (1), 139–153.

Sadrossadat, E., Heidaripanah, A., and Osouli, S., 2016. Prediction of the resilient modulus of flexible pavement subgrade soils using adaptive neuro-fuzzy inference systems. *Construction and Building Materials*, 123, 235–247.

Saptoro, A., Tadé, M.O., and Vuthaluru, H., 2012. A modified Kennard-Stone algorithm for optimal division of data for developing artificial neural network models. *Chemical Product and Process Modeling*, 7 (1).

Sarkhani Benemaran, R., Esmaeili-Falak, M., and Katebi, H., 2021. Physical and numerical modelling of pile-stabilised saturated layered slopes. *Proceedings of the Institution of Civil Engineers: Geotechnical Engineering*, 1–16.

Seed, H.B., Chan, C.K., and Lee, C.E., 1962. Resilience characteristics of subgrade soils and their relation to fatigue failures in asphalt pavements. *In*: *International Conference on the Structural Design of Asphalt Pavements. SupplementUniversity of Michigan, Ann Arbor*.

Shafabakhsh, G. and Tanakizadeh, A., 2015. Investigation of loading features effects on resilient modulus of asphalt mixtures using Adaptive Neuro-Fuzzy Inference System. *Construction and Building Materials*, 76, 256–263.

Shahin, M.A., Maier, H.R., and Jaksa, M.B., 2004. Data division for developing neural networks applied to geotechnical engineering. *journal of Computing in Civil Engineering*, 18 (2), 105–114.

Shi, Y. and Eberhart, R.C., 1998. Parameter selection in particle swarm optimization. *In*: *International conference on evolutionary programming*. Springer, 591–600.

Titi, H.H. and Matar, M.G., 2018. Estimating resilient modulus of base aggregates for mechanistic-empirical pavement design and performance evaluation. *Transportation Geotechnics*, 17, 141–153.

Trelea, I.C., 2003. The particle swarm optimization algorithm: convergence analysis and parameter selection. *Information processing letters*, 85 (6), 317–325.

Uzan, J., 1985. Characterization of granular material. *Transportation research record*, 1022 (1), 52–59.

Xue, X., 2018. Evaluation of concrete compressive strength based on an improved PSO-LSSVM model. *Computers and Concrete*, 21 (5), 505–511.

Yan, K., Xu, H., and Shen, G., 2014. Novel approach to resilient modulus using routine subgrade soil properties. *International Journal of Geomechanics*, 14 (6), 4014025.

Yang, M., Tao, B., Chen, C., Jia, W., Sun, S., Zhang, T., and Wang, X., 2019. Machine learning models based on molecular fingerprints and an extreme gradient boosting method lead to the discovery of JAK2 inhibitors. *Journal of chemical information and modeling*, 59 (12), 5002–5012.

Zaman, M., Solanki, P., Ebrahimi, A., and White, L., 2010. Neural network modeling of resilient modulus using routine subgrade soil properties. *International Journal of*

Geomechanics, 10 (1), 1–12.

Zhang, W., Wu, C., Zhong, H., Li, Y., and Wang, L., 2021. Prediction of undrained shear strength using extreme gradient boosting and random forest based on Bayesian optimization. *Geoscience Frontiers*, 12 (1), 469–477.

Zhou, J., Li, E., Wang, M., Chen, X., Shi, X., and Jiang, L., 2019. Feasibility of stochastic gradient boosting approach for evaluating seismic liquefaction potential based on SPT and CPT case histories. *Journal of Performance of Constructed Facilities*, 33 (3), 4019024.

Zhou, J., Li, E., Yang, S., Wang, M., Shi, X., Yao, S., and Mitri, H.S., 2019. Slope stability prediction for circular mode failure using gradient boosting machine approach based on an updated database of case histories. *Safety Science*, 118, 505–518.

Tables:

Table 1. Summary of the previous studies on predicting the M_R of flexible pavement foundations

Reference	Year	Inputs	Model	Data	R^2	RMSE
(Hanittinan 2007)	2007	$P\#200, PI, LL, \sigma_o, \sigma_d, S_r, \omega_{opt}, \omega_c, and\ q_u$	ANN	(Kim 1999, 2004, Huang 2001, Rodgers 2006)	0.978	-
(Park *et al.* 2009)	2009	$\gamma_d, C_u, P\#200, PI, \sigma_o, \sigma_d, and\ \omega_{opt}$	ANN	(Park *et al.* 2009)	0.937	-
(Zaman *et al.* 2010)	2010	$\omega_c, \gamma_d, PI, P\#200, q_u, \sigma_d, and\ \theta$	RBFNN	(Ebrahimi 2006)	0.6284	-
(Yan *et al.* 2014)	2014	$\omega_c, \gamma_d, PI, P\#200, q_u, \sigma_d, and\ \theta$	GEP	(Ebrahimi 2006)	0.7815	-
(Pal and Deswal 2014)	2014	$P\#200, PI, LL, \sigma_o, \sigma_d, S_r, \omega_{opt}, \omega_c, and\ q_u$	ELM	(Kim 1999, 2004, Huang 2001, Rodgers 2006)	0.982	3.47
(Sadrossadat *et al.* 2016)	2016	$P\#200, PI, LL, \sigma_o, \sigma_d, S_r, \omega_{opt}, \omega_c, and\ q_u$	ANFIS	(Kim 1999, 2004, Huang 2001, Rodgers 2006)	0.974	4.85
(Chou *et al.* 2016)	2016	$\gamma_d, C_u, P\#200, PI, \sigma_o, \sigma_d, and\ \omega_{opt}$	SFA-LSSVR	(Park *et al.* 2009)	0.9216	14.77
(Sadrossadat *et al.* 2018)	2018	$P\#200, PI, LL, \sigma_o, \sigma_d, S_r, \omega_{opt}, \omega_c, and\ q_u$	LGP	(Kim 1999, 2004, Huang 2001, Rodgers 2006)	0.8649	11.91
(Ghorbani *et al.* 2020)	2020	$P\#200, PI, LL, \sigma_o, \sigma_d, S_r, \omega_{opt}, \omega_c, and\ q_u$	ANN-GA	(Kim 1999, 2004, Huang 2001, Rodgers 2006)	0.97	5.5
(Kayadelen *et al.* 2021)	2021	$P\#200, PI, LL, \sigma_o, \sigma_d, S_r, \omega_{opt}, \omega_c, and\ q_u$	RF	(Kim 1999, 2004, Huang 2001, Rodgers 2006)	0.9801	4.6
(Heidarabadizadeh *et al.* 2021)	2021	$\gamma_d, C_u, P\#200, PI, \sigma_o, \sigma_d, and\ \omega_{opt}$	SVM-CBO	(Park *et al.* 2009)	0.9978	3.1348
(Kayadelen *et al.* 2021)	2021	$\gamma_d, C_u, P\#200, PI, \sigma_o, \sigma_d, and\ \omega_{opt}$	RF	(Park *et al.* 2009)	0.9409	16.85
(Kayadelen *et al.* 2021)	2021	$\gamma_d, C_u, P\#200, PI, \sigma_o, \sigma_d, and\ \omega_{opt}$	M5P-Tree	(Park *et al.* 2009)	0.91	30.37
(Kayadelen *et al.* 2021)	2021	$P\#200, PI, LL, \sigma_o, \sigma_d, S_r, \omega_{opt}, \omega_c, and\ q_u$	M5P-Tree	(Kim 1999, 2004, Huang 2001, Rodgers 2006)	0.97	6.71

*ANFIS = Adaptive Neuro-Fuzzy Inference System, ELM= Extreme Learning Machine, ANN = Artificial Neural Network, GA = Genetic Algorithm, RF = Random Forests, LGP= Linear Genetic Programming, SVM= Support Vector Machine, CBO= Colliding Bodies Optimization, SFA= Smart Firefly Algorithm, LSSVR= Least Square Support Vector Regression, GEP=Genetic Programming, RBFNN=Radial Basis Function Neural Network, γ_d= Dry Density, C_u= Uniformity Coefficient, θ= Bulk Stress.

Table 2. The statistical parameters of the input and output variables in the training and testing datasets

Model variables and datasets	Statistical parameters										
	Min.	Max.	Avg.	St. D.	Med.	Skew.	Mode	Kurt.	Range	S. Var.	St. E.
Passing a No. 200 sieve (#200) (%)											
Training data	42	100	75.18	17.582	76	-0.0178	100	-1.3332	58	308.66	0.6803
Testing data	42	100	75.336	17.872	76	-0.0095	100	-1.427	58	317.96	1.1968
Liquid limit (%)											
Training data	21	59	32.83	10.072	29	1.444	26	1.2008	38	101.29	0.3897
Testing data	21	59	31.926	9.444	29	1.4306	26	1.478	38	88.789	0.6324
Plasticity index (%)											
Training data	2	36	12.79	8.7912	11	1.4924	11	1.36824	34	77.17	0.3401
Testing data	2	36	12.3605	8.3844	10	1.5192	9	1.8119	34	69.983	0.5615
Optimum water content (%)											
Training data	9.4	24.2	15.22	3.0689	14.4	1.274	14	2.13067	14.8	9.4045	0.1187
Testing data	9.4	24.2	15.084	2.9145	14.4	0.8985	14	1.6432	14.8	8.4562	0.1952
Water content (%)											
Training data	7.53	27.2	15.37	3.523	14.92	0.866	16	1.57912	19.67	12.393	0.1363
Testing data	7.53	27.2	15.228	3.5561	14.72	0.8193	13.8	1.0986	19.67	12.589	0.2381
Degree of saturation (%)											
Training data	42.92	100	81.51	11.399	83.8	-0.694	89.57	0.13506	57.08	129.75	0.441
Testing data	46.1	100	81.208	10.477	83.19	-0.4246	79.3	-0.0008	53.9	109.27	0.7016
Unconfined compressive strength (kPa)											
Training data	54.3	715.7	307.4	158.865	292.3	0.7776	302.68	0.0007	661.44	25200	6.1467
Testing data	54.3	715.74	322.31	173.94	302.68	0.6311	102.7	-0.4029	661.44	30118	11.648
Confining stress (kPa)											
Training data	0	41.4	20.95	16.411	20.69	-0.034	20.69	-1.4243	41.4	268.92	0.635
Testing data	0	41.4	21.032	16.232	20.69	-0.02	20.69	-1.3958	41.4	262.28	1.0869
Deviatoric stress (kPa)											
Training data	11	71.22	39.8	17.886	41.37	0.0528	41.37	-1.074	60.22	319.43	0.692
Testing data	10	71.69	41.843	19.158	41.37	-0.0965	41.37	-1.2232	61.69	365.4	1.2829
Resilient modulus (MPa)											
Training data	6.4	151.6	54.29	29.842	52.185	0.313	14.1	-0.7448	145.22	889.21	1.1546
Testing data	7.9	179.44	56.41	29.199	56.3	0.5609	11.9	0.7237	171.54	848.75	1.9553

* Min. = Minimum, Max. = Maximum, Avg. = Average, St. D. = Standard Deviation, Med. = Median, Skew. = Skewness, Kurt. = Kurtosis, S. Var. = Sample Variance, St. E. = Standard Error

Table 3. The parameters of the models and the optimal parameters

Method	Parameters	Value	Optimal parameter	Value
PSO	Cognitive coefficient 1 ($C1$)	2	$num\_boosting\_rounds$	67
	Cognitive coefficient 2 ($C2$)	2	eta	0.1153
	Maximum velocity (V_{max})	5	$lambda$	0.02
	Maximum inertia weight (W_{max})	0.9		
	Minimum inertia weight (W_{min})	0.2		
SCA	a	2	$num\_boosting\_rounds$	88
			eta	0.0932
			$lambda$	0.02
MVO	Maximum of Wormhole existence probability	1	$num\_boosting\_rounds$	115
	Minimum of wormhole existence probability	0.2	eta	0.1305
			$lambda$	3.15
SSO	Upper female percent	90	$num\_boosting\_rounds$	79
	Lower female percent	70	eta	0.928
	Probabilities of attraction or repulsion	0.7	$lambda$	0.0217

Table 4. Comparison of models' performance

Model	R^2	Score	RMSE	Score	MAE	Score	PI	Score	VAF	Score	A_{10}-index	Score	Total score
	Training data												
SSO-XGB	0.9918	4	2.7047	4	2.0742	2	0.025	4	99.1774	4	0.8219	1	19
SCA-XGB	0.9895	1	3.2041	1	2.2765	1	0.0296	1	98.942	1	0.8458	2	7
MVO-XGB	0.9909	2	2.8569	2	2.0401	3	0.0264	2	99.0877	2	0.8578	4	15
PSO-XGB	0.9911	3	2.8306	3	2.0218	4	0.0261	3	99.1019	3	0.8533	3	19
	Testing data												
SSO-XGB	0.9642	1	5.6047	1	4.143	1	0.0501	1	96.4178	1	0.6682	1	6
SCA-XGB	0.9745	4	5.0612	2	3.4928	2	0.0452	2	97.3785	4	0.7354	2	16
MVO-XGB	0.9732	2	4.8897	3	3.3328	3	0.0436	3	97.2946	2	0.7802	3	16
PSO-XGB	0.9736	3	4.8442	4	3.2966	4	0.0432	4	97.3433	3	0.7803	4	22

Table 5. Comprising the efficiency of the proposed model against the previous studies

Reference	Inputs	Model	Data	R^2	RMSE
This study	$P\#200, PI, LL, \sigma_o, \sigma_d, S_r, \omega_{opt}, \omega_c, and\ q_u$	PSO-XGB	(Kim 1999, 2004, Huang 2001, Rodgers 2006)	**0.9911**	**2.8306**
(Hanittinan 2007)	$P\#200, PI, LL, \sigma_o, \sigma_d, S_r, \omega_{opt}, \omega_c, and\ q_u$	ANN	(Kim 1999, 2004, Huang 2001, Rodgers 2006)	0.978	-
(Pal and Deswal 2014)	$P\#200, PI, LL, \sigma_o, \sigma_d, S_r, \omega_{opt}, \omega_c, and\ q_u$	ELM	(Kim 1999, 2004, Huang 2001, Rodgers 2006)	0.982	3.47
(Sadrossadat *et al.* 2016)	$P\#200, PI, LL, \sigma_o, \sigma_d, S_r, \omega_{opt}, \omega_c, and\ q_u$	ANFIS	(Kim 1999, 2004, Huang 2001, Rodgers 2006)	0.974	4.85
(Ghorbani *et al.* 2020)	$P\#200, PI, LL, \sigma_o, \sigma_d, S_r, \omega_{opt}, \omega_c, and\ q_u$	ANN-GA	(Kim 1999, 2004, Huang 2001, Rodgers 2006)	0.97	5.5
(Kayadelen *et al.* 2021)	$P\#200, PI, LL, \sigma_o, \sigma_d, S_r, \omega_{opt}, \omega_c, and\ q_u$	RF	(Kim 1999, 2004, Huang 2001, Rodgers 2006)	0.9801	4.6
(Kayadelen *et al.* 2021)	$P\#200, PI, LL, \sigma_o, \sigma_d, S_r, \omega_{opt}, \omega_c, and\ q_u$	M5P-Tree	(Kim 1999, 2004, Huang 2001, Rodgers 2006)	0.97	6.71
(Sadrossadat *et al.* 2018)	$P\#200, PI, LL, \sigma_o, \sigma_d, S_r, \omega_{opt}, \omega_c, and\ q_u$	LGP	(Kim 1999, 2004, Huang 2001, Rodgers 2006)	0.8649	11.91
(Park *et al.* 2009)	$\gamma_d, C_u, P\#200, PI, \sigma_o, \sigma_d, and\ \omega_{opt}$	ANN	(Park *et al.* 2009)	0.937	-
(Zaman *et al.* 2010)	$\omega_c, \gamma_d, PI, P\#200, q_u, \sigma_d, and\ \theta$	RBFNN	(Ebrahimi 2006)	0.6284	-
(Yan *et al.* 2014)	$\omega_c, \gamma_d, PI, P\#200, q_u, \sigma_d, and\ \theta$	GEP	(Ebrahimi 2006)	0.7815	-
(Chou *et al.* 2016)	$\gamma_d, C_u, P\#200, PI, \sigma_o, \sigma_d, and\ \omega_{opt}$	SFA-LSSVR	(Park *et al.* 2009)	0.9216	14.77
(Heidarabadizadeh *et al.* 2021)	$\gamma_d, C_u, P\#200, PI, \sigma_o, \sigma_d, and\ \omega_{opt}$	SVM-CBO	(Park *et al.* 2009)	0.9978	3.1348
(Kayadelen *et al.* 2021)	$\gamma_d, C_u, P\#200, PI, \sigma_o, \sigma_d, and\ \omega_{opt}$	RF	(Park *et al.* 2009)	0.9409	16.85
(Kayadelen *et al.* 2021)	$\gamma_d, C_u, P\#200, PI, \sigma_o, \sigma_d, and\ \omega_{opt}$	M5P-Tree	(Park *et al.* 2009)	0.91	30.37

Table 6. Sensitivity analysis using the R^2 and RMSE indexes on the PSO-XGB model

Index	PSO-XGB	Removed parameter								
		P#200	LL	PI	σ_o	σ_d	S_r	ω_{opt}	ω_c	q_u
R^2	0.9736	0.9720	0.9715	0.9759	**0.7299**	0.9076	0.9627	0.973	0.9731	0.9723
RMSE (MPa)	4.8442	5.0211	5.0161	4.6656	**15.1808**	**8.9107**	5.7060	4.9876	4.9696	5.1378

Figures:

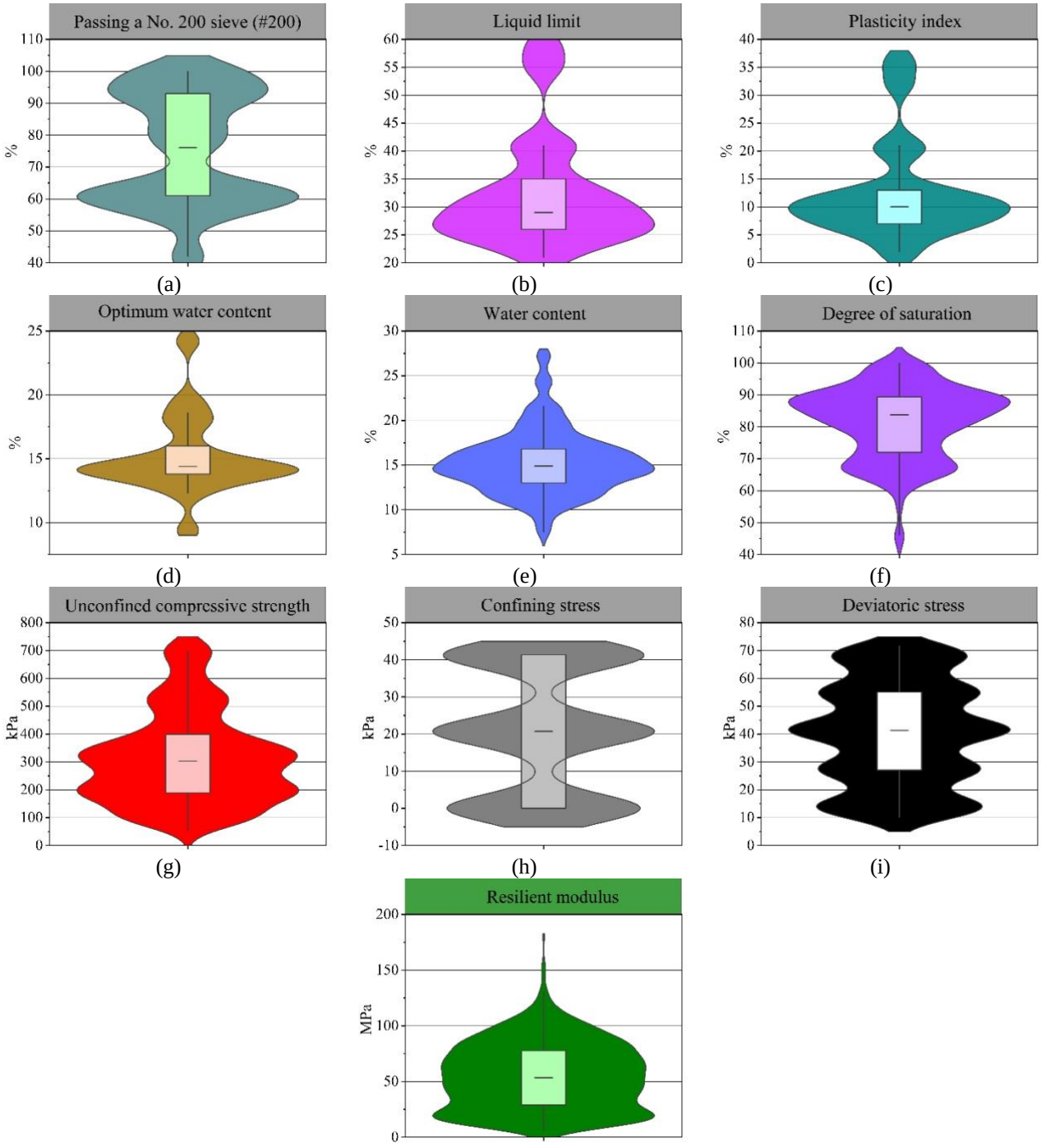

Fig. 1. Violin plots distribution of M_R data

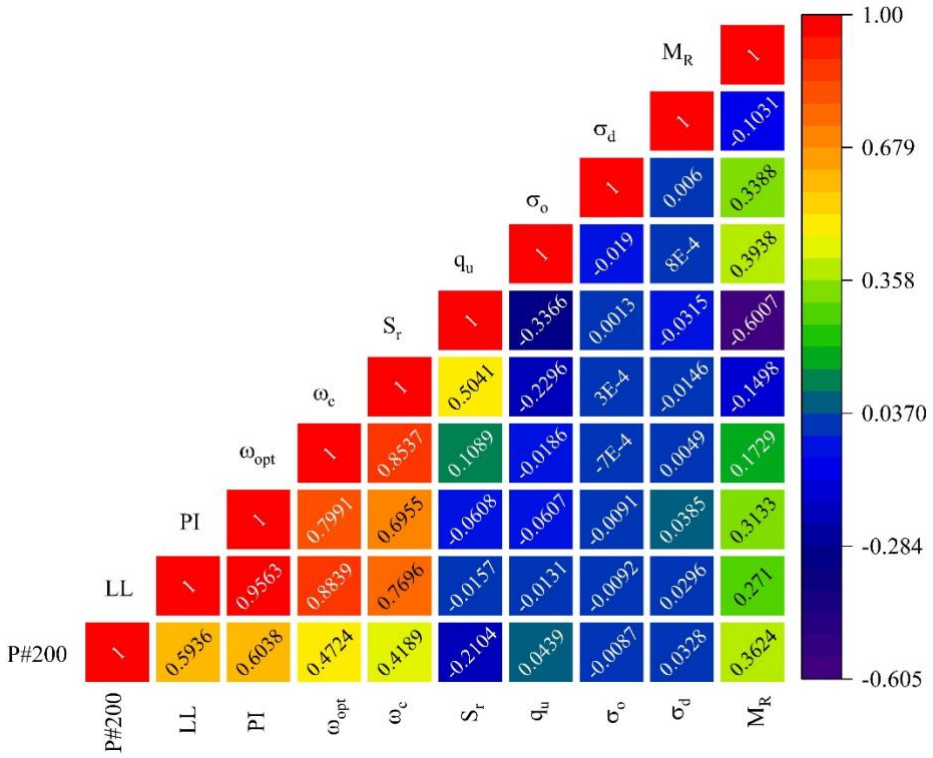

Fig. 2. PCC between the variables

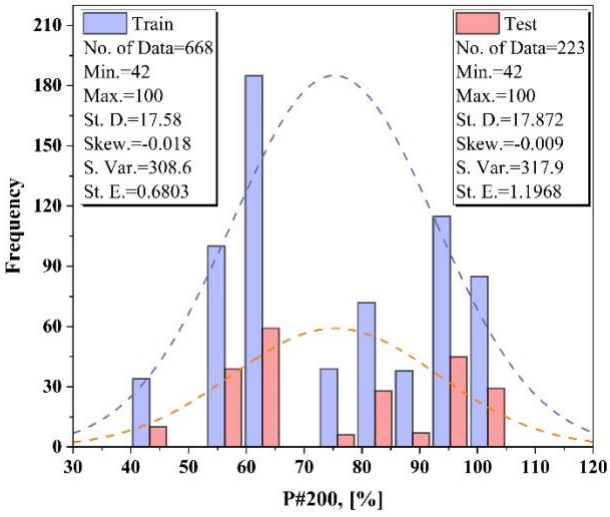

(a)

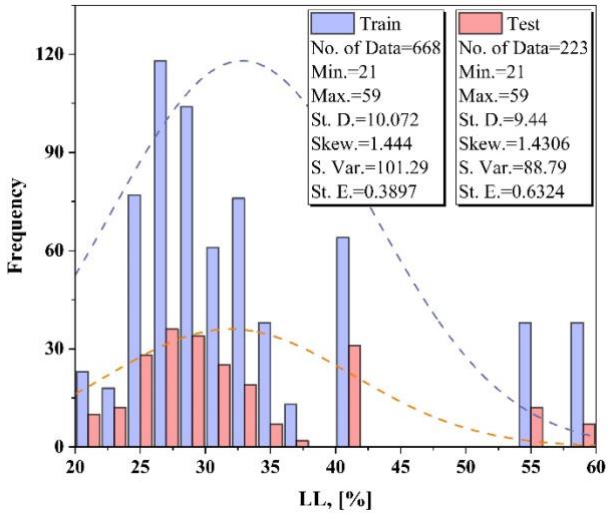

(b)

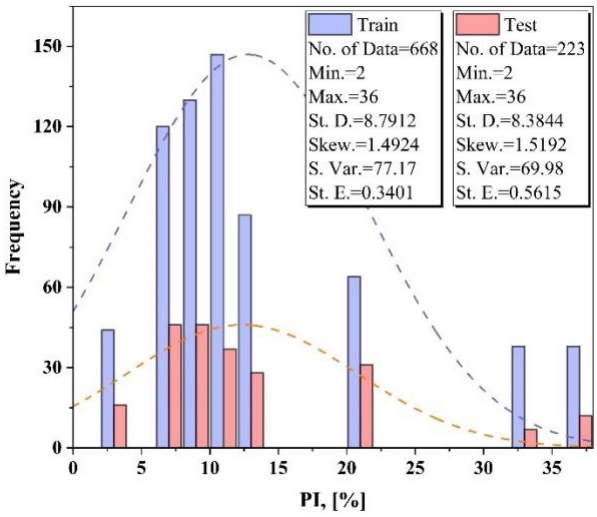
Train
No. of Data=668
Min.=2
Max.=36
St. D.=8.7912
Skew.=1.4924
S. Var.=77.17
St. E.=0.3401
Test
No. of Data=223
Min.=2
Max.=36
St. D.=8.3844
Skew.=1.5192
S. Var.=69.98
St. E.=0.5615
Frequency
PI, [%]

(c)

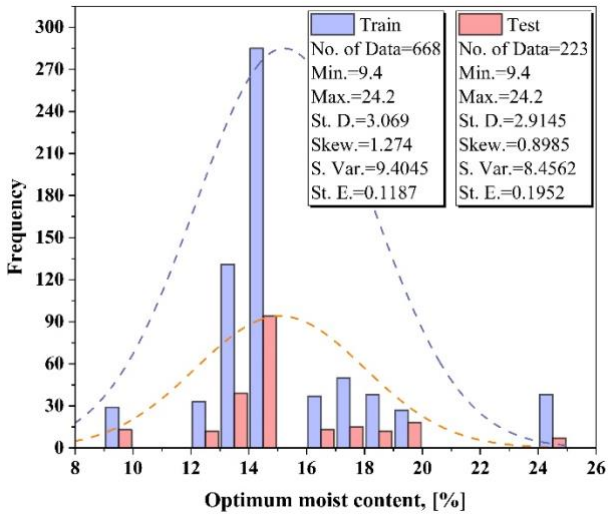
Train
No. of Data=668
Min.=9.4
Max.=24.2
St. D.=3.069
Skew.=1.274
S. Var.=9.4045
St. E.=0.1187
Test
No. of Data=223
Min.=9.4
Max.=24.2
St. D.=2.9145
Skew.=0.8985
S. Var.=8.4562
St. E.=0.1952
Frequency
Optimum moist content, [%]

(d)

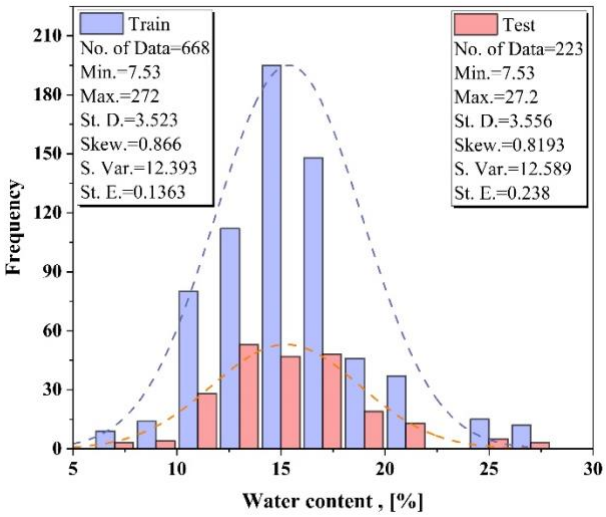
Train
No. of Data=668
Min.=7.53
Max.=272
St. D.=3.523
Skew.=0.866
S. Var.=12.393
St. E.=0.1363
Test
No. of Data=223
Min.=7.53
Max.=27.2
St. D.=3.556
Skew.=0.8193
S. Var.=12.589
St. E.=0.238
Frequency
Water content , [%]

(e)

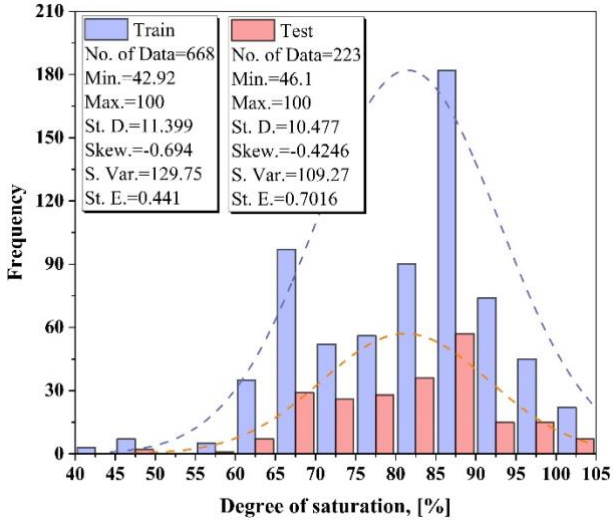
Train
No. of Data=668
Min.=42.92
Max.=100
St. D.=11.399
Skew.=-0.694
S. Var.=129.75
St. E.=0.441
Test
No. of Data=223
Min.=46.1
Max.=100
St. D.=10.477
Skew.=-0.4246
S. Var.=109.27
St. E.=0.7016
Frequency
Degree of saturation, [%]

(f)

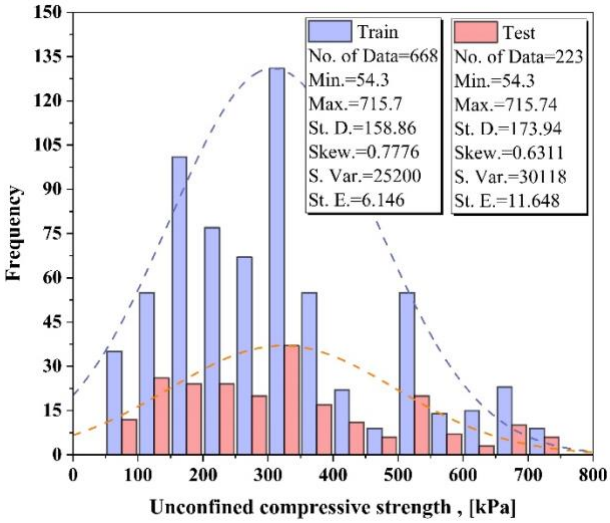
Train
No. of Data=668
Min.=54.3
Max.=715.7
St. D.=158.86
Skew.=0.7776
S. Var.=25200
St. E.=6.146
Test
No. of Data=223
Min.=54.3
Max.=715.74
St. D.=173.94
Skew.=0.6311
S. Var.=30118
St. E.=11.648
Frequency
Unconfined compressive strength , [kPa]

(g)

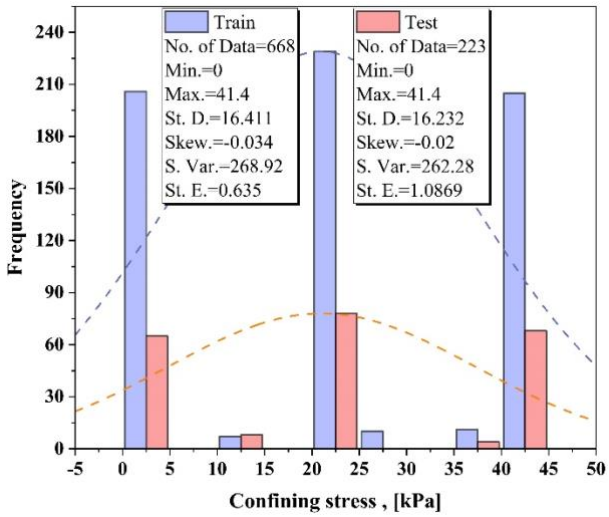
Train
No. of Data=668
Min.=0
Max.=41.4
St. D.=16.411
Skew.=-0.034
S. Var.=268.92
St. E.=0.635
Test
No. of Data=223
Min.=0
Max.=41.4
St. D.=16.232
Skew.=-0.02
S. Var.=262.28
St. E.=1.0869
Frequency
Confining stress , [kPa]

(h)

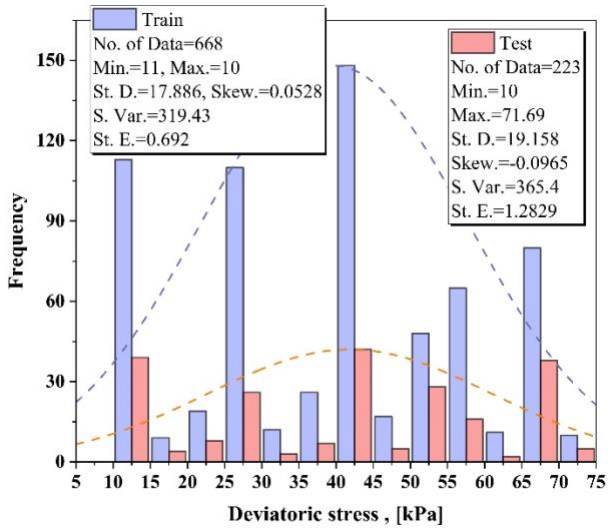

(i)

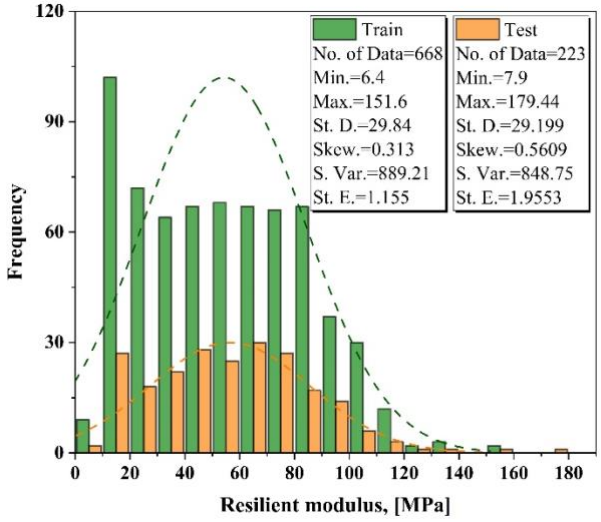

(j)

Fig. 3. Histograms of variables and their normal distribution plots for training and testing data

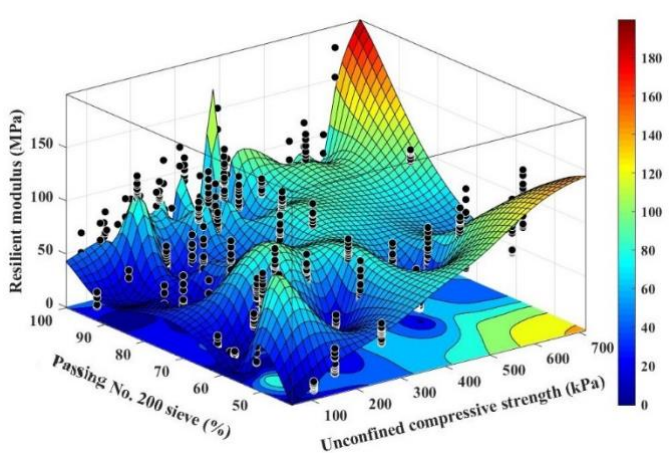

(a)

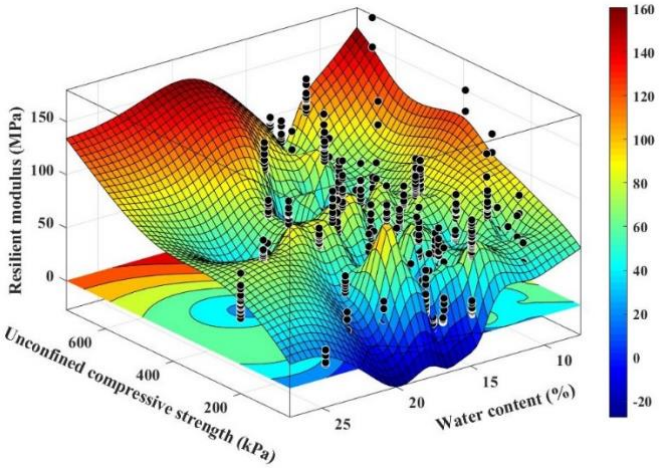

(b)

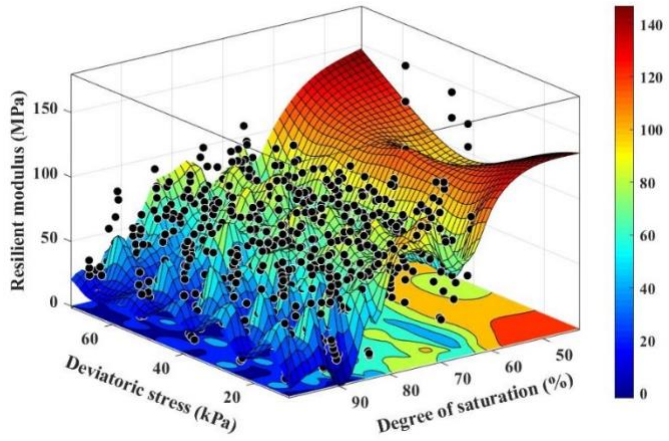

(c)

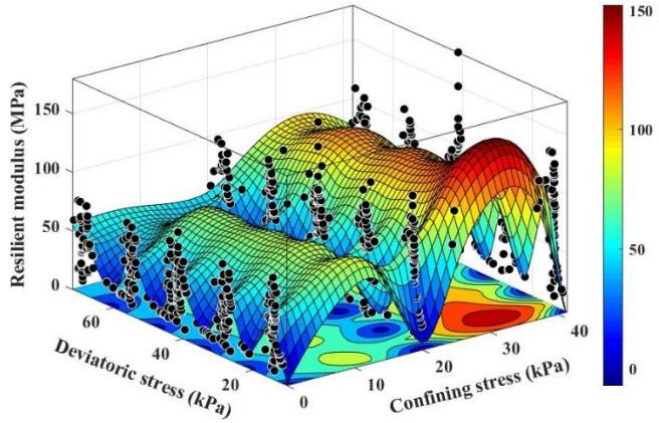

(d)

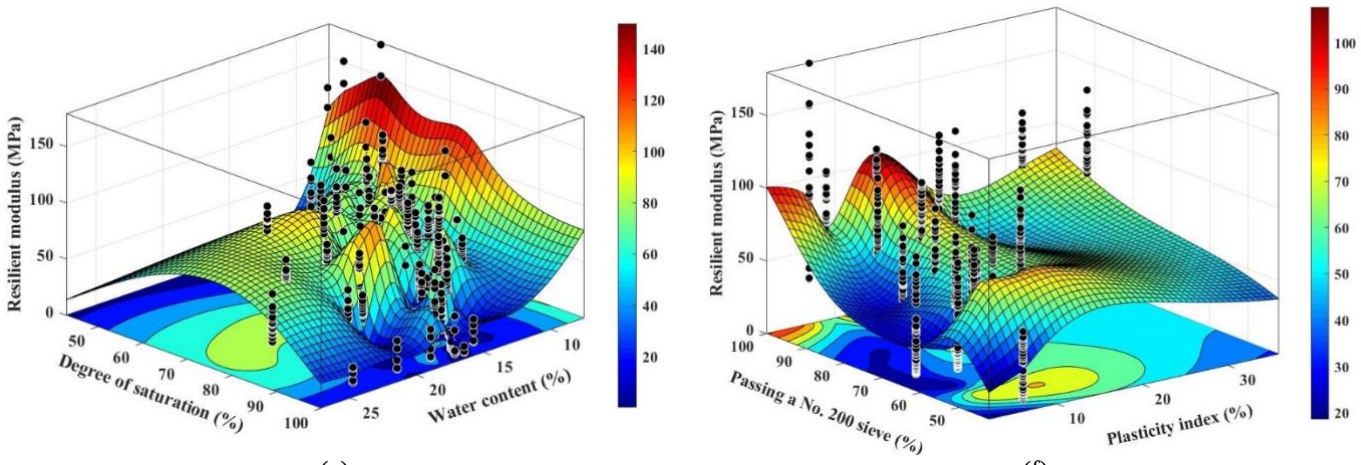

(e) (f)

Fig. 4. Surface plots of M_R versus input variables

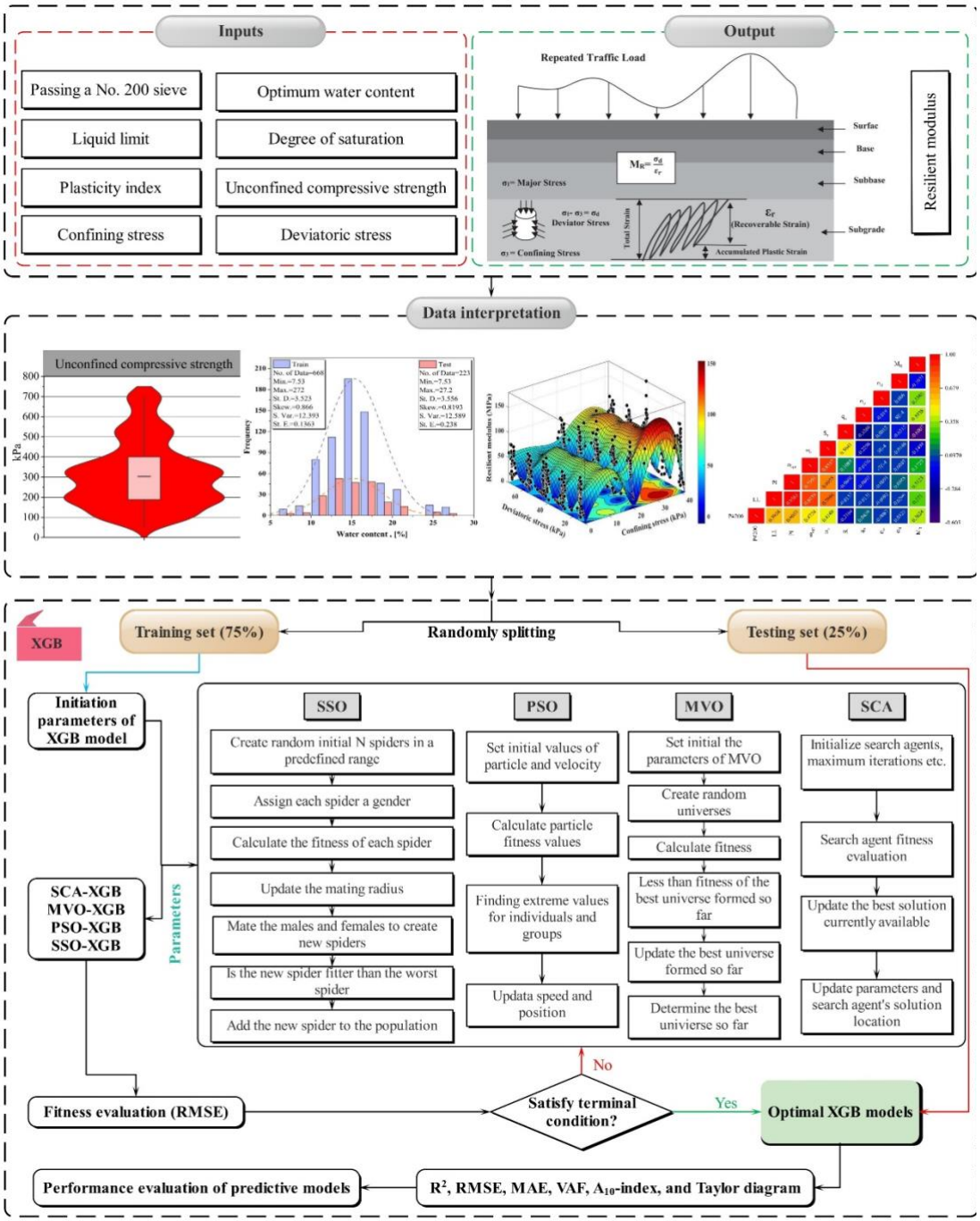

Fig. 5. The overall analysis process of the XGB models

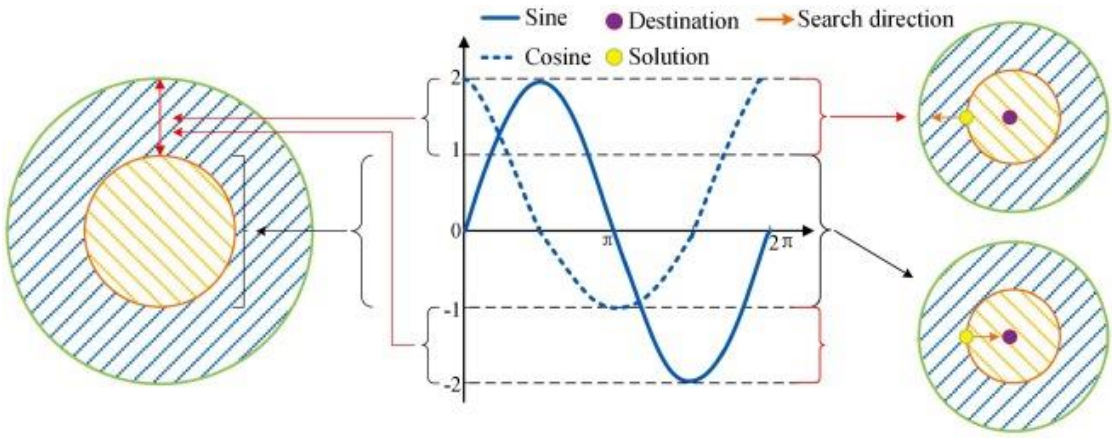

Fig. 6. Sketch map of the SCA search principle (Feng *et al.* 2020)

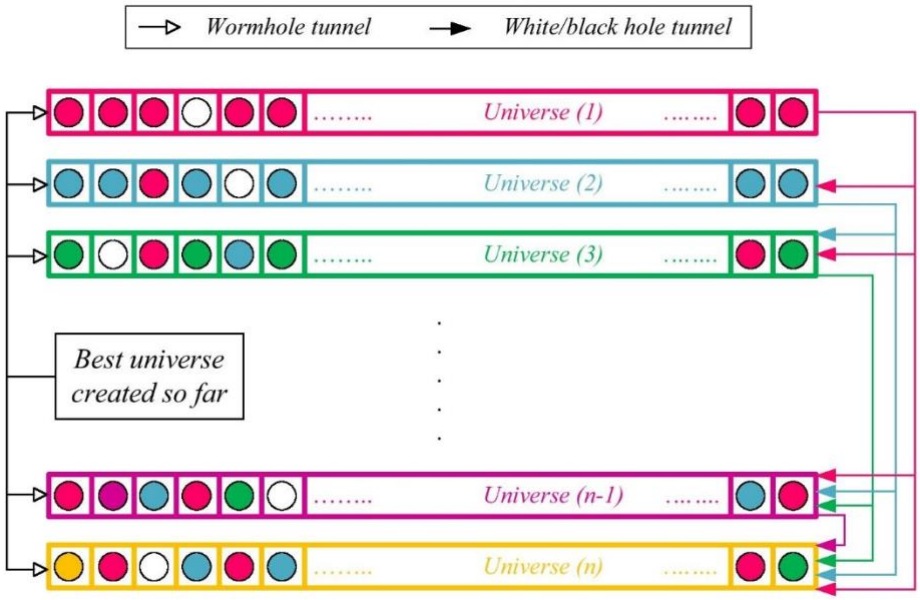

Fig. 7. Basic idea of a MVO algorithm (Mirjalili *et al.* 2016)

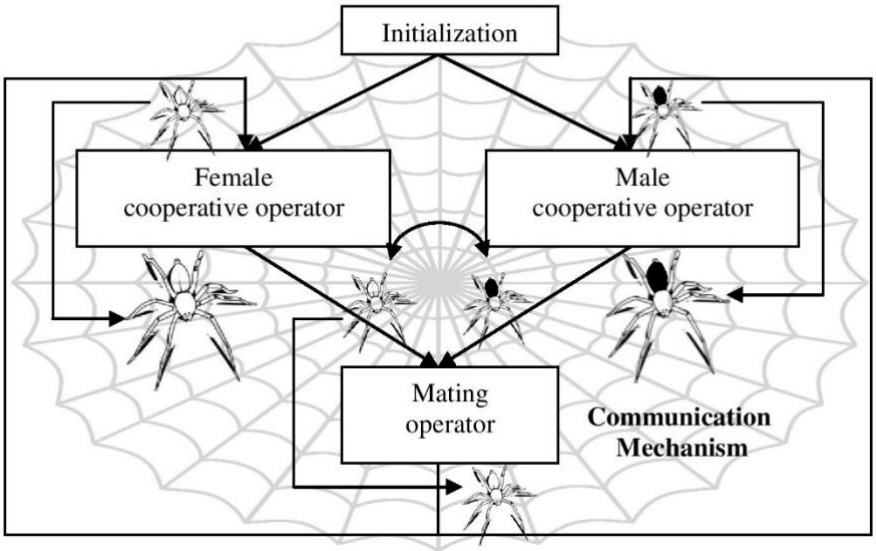

Fig. 8. Schematic representation of the SSO (Cuevas *et al.* 2013)

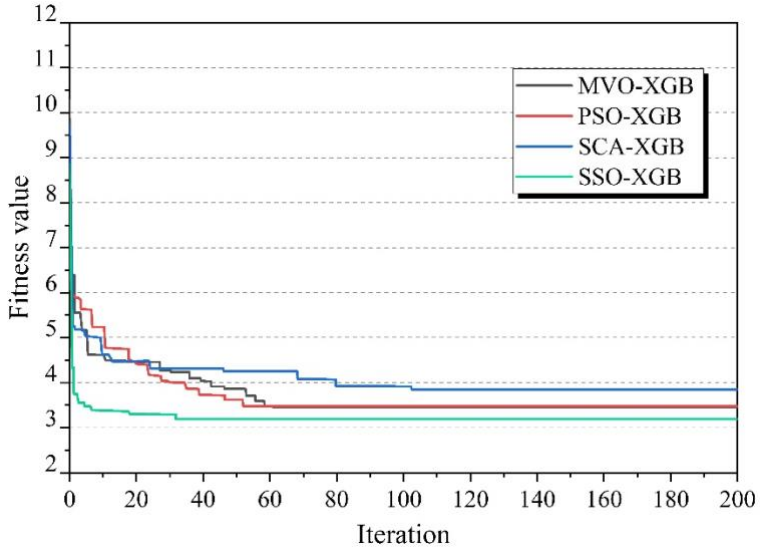

Fig. 9. The fitness reduction in the optimization process

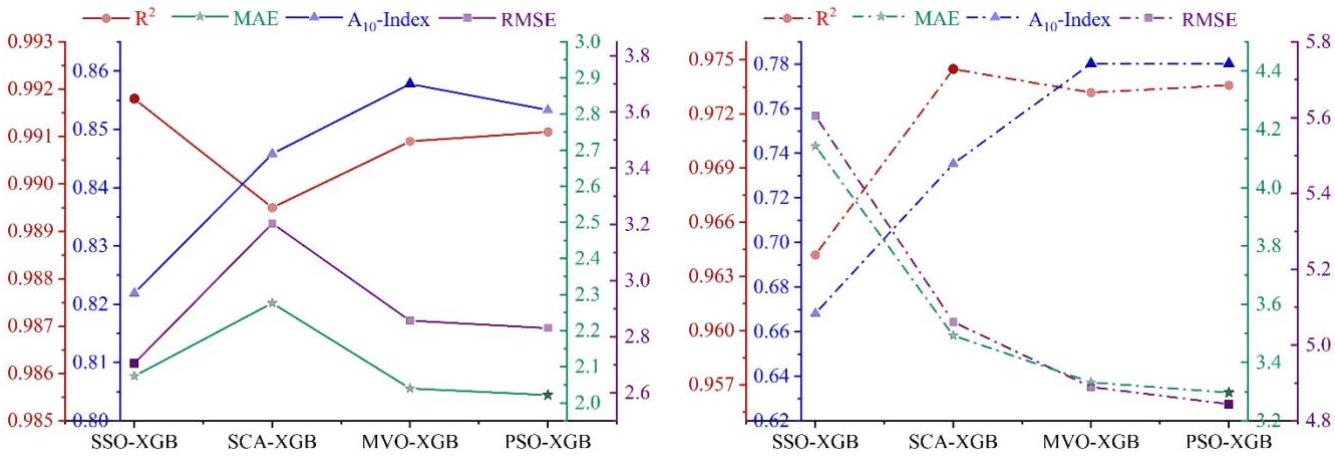

(a) (b)

Fig. 10. Multi-axis figure of model assessment evaluators: (a) Train, (b) Test

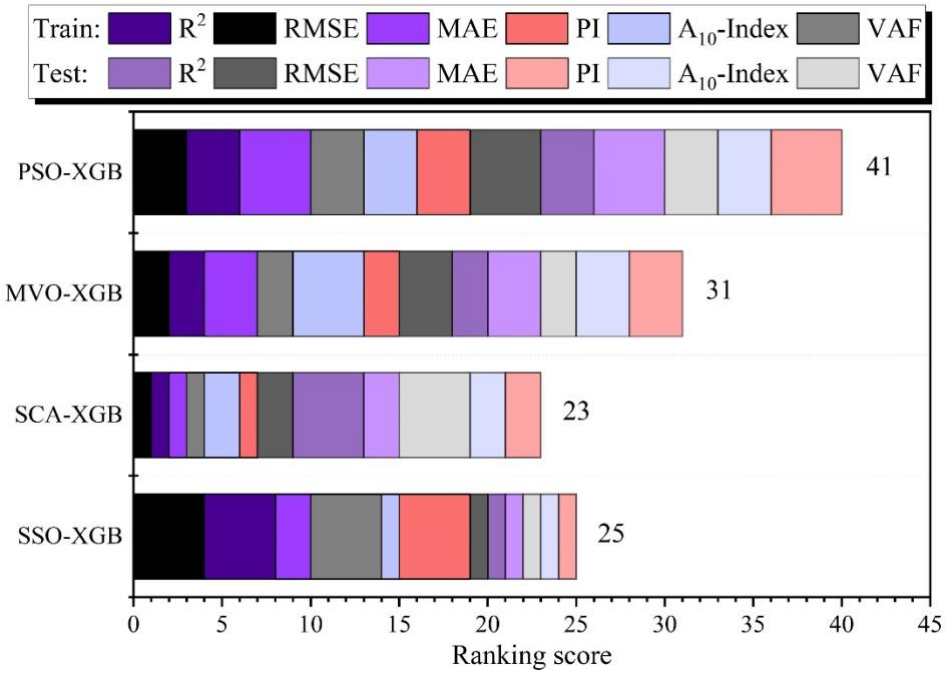

Fig. 11. Intuitive presentation of accumulated ranking of developed models

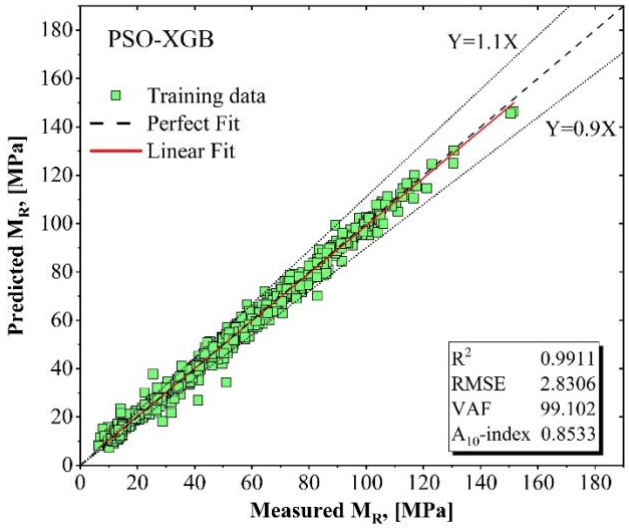

(a)

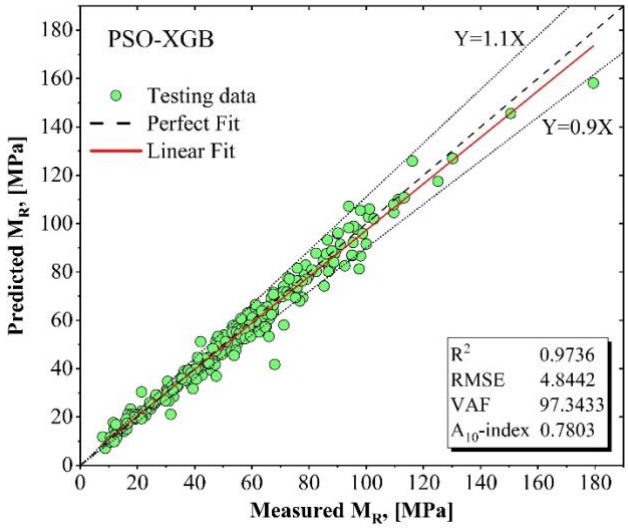

(b)

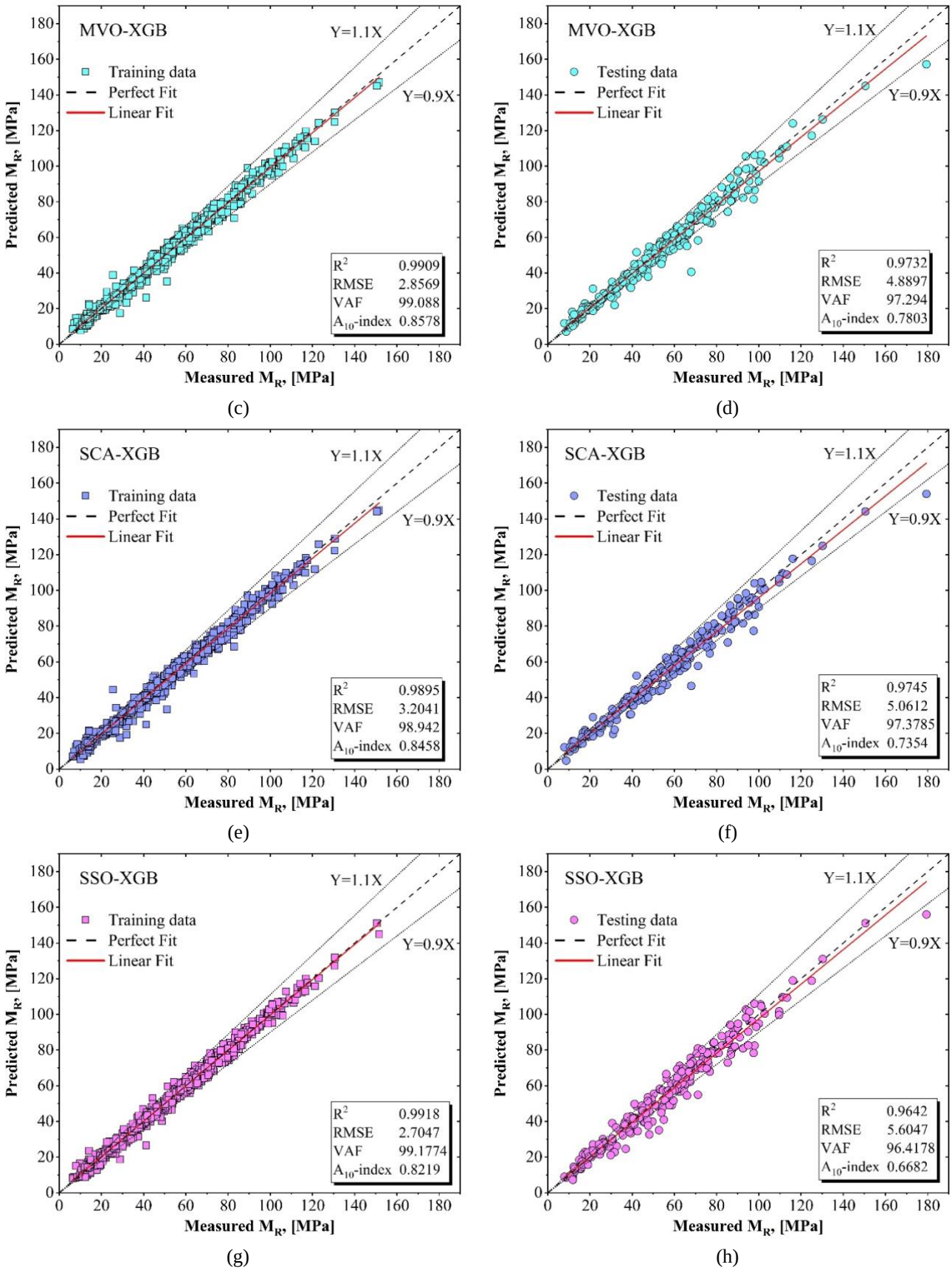

Fig. 12. Correlation between measured and predicted values of M_R

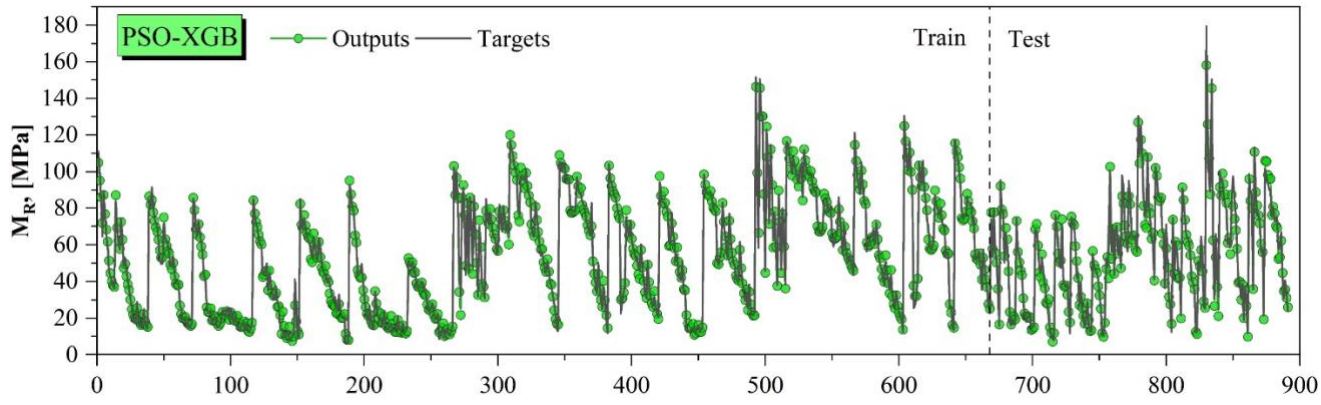

(a)

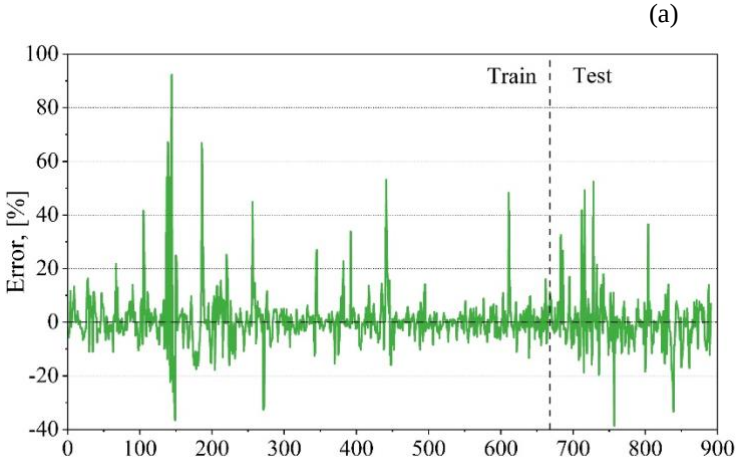

(b)

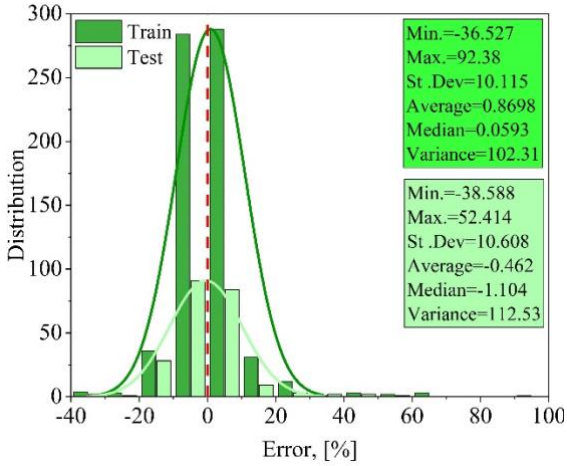

(c)

Fig. 13. Results of the developed PSO-XGB model in predicting M_R

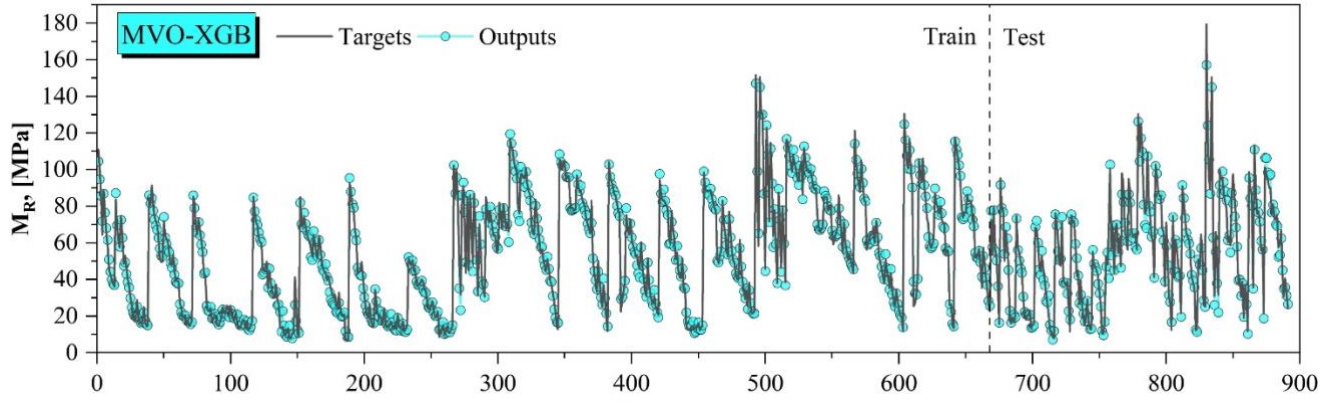

(a)

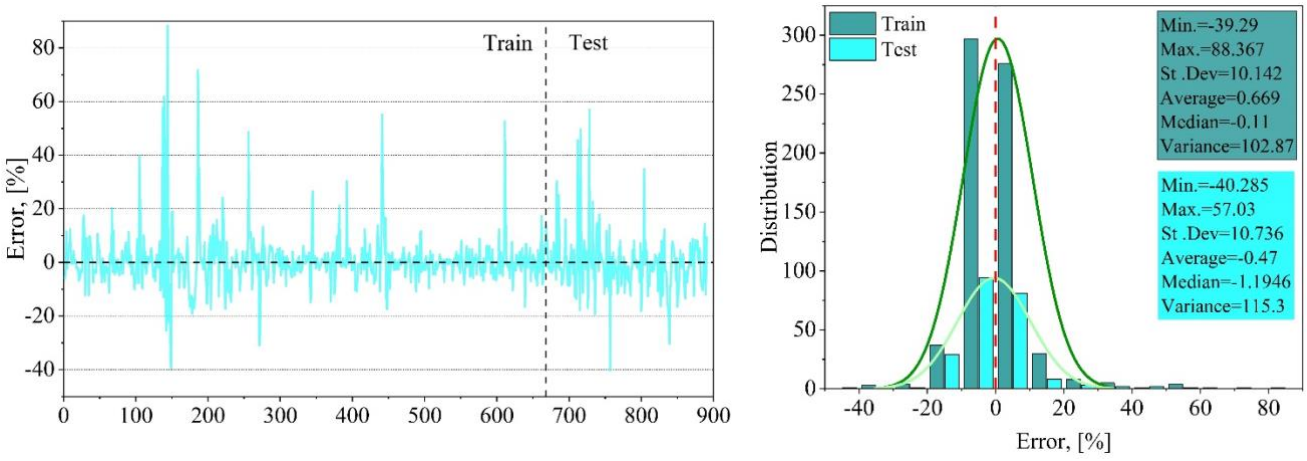

(b) (c)

Fig. 14. Results of the developed MVO-XGB model in predicting M_R

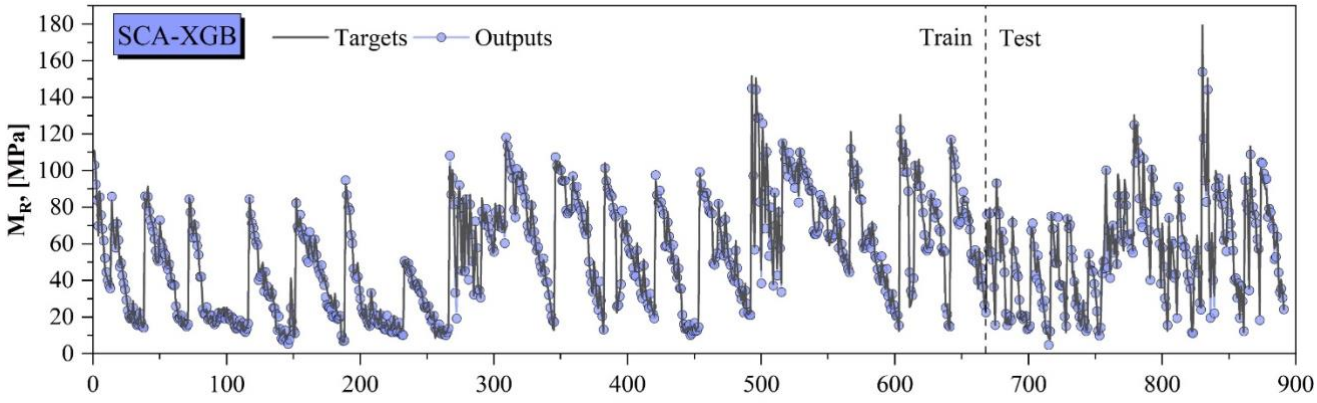

(a)

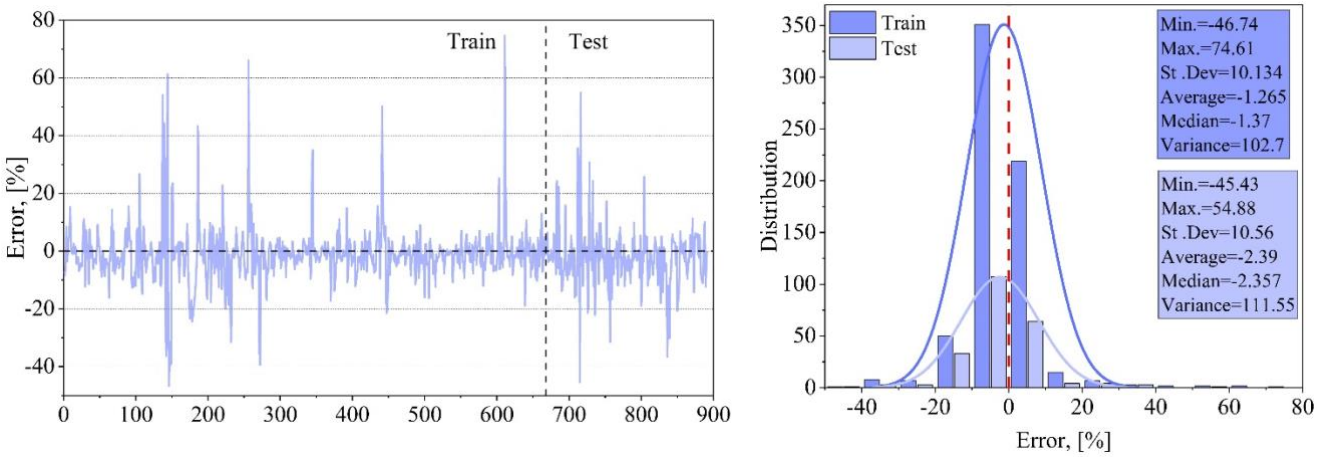

(b) (c)

Fig. 15. Results of the developed SCA-XGB model in predicting M_R

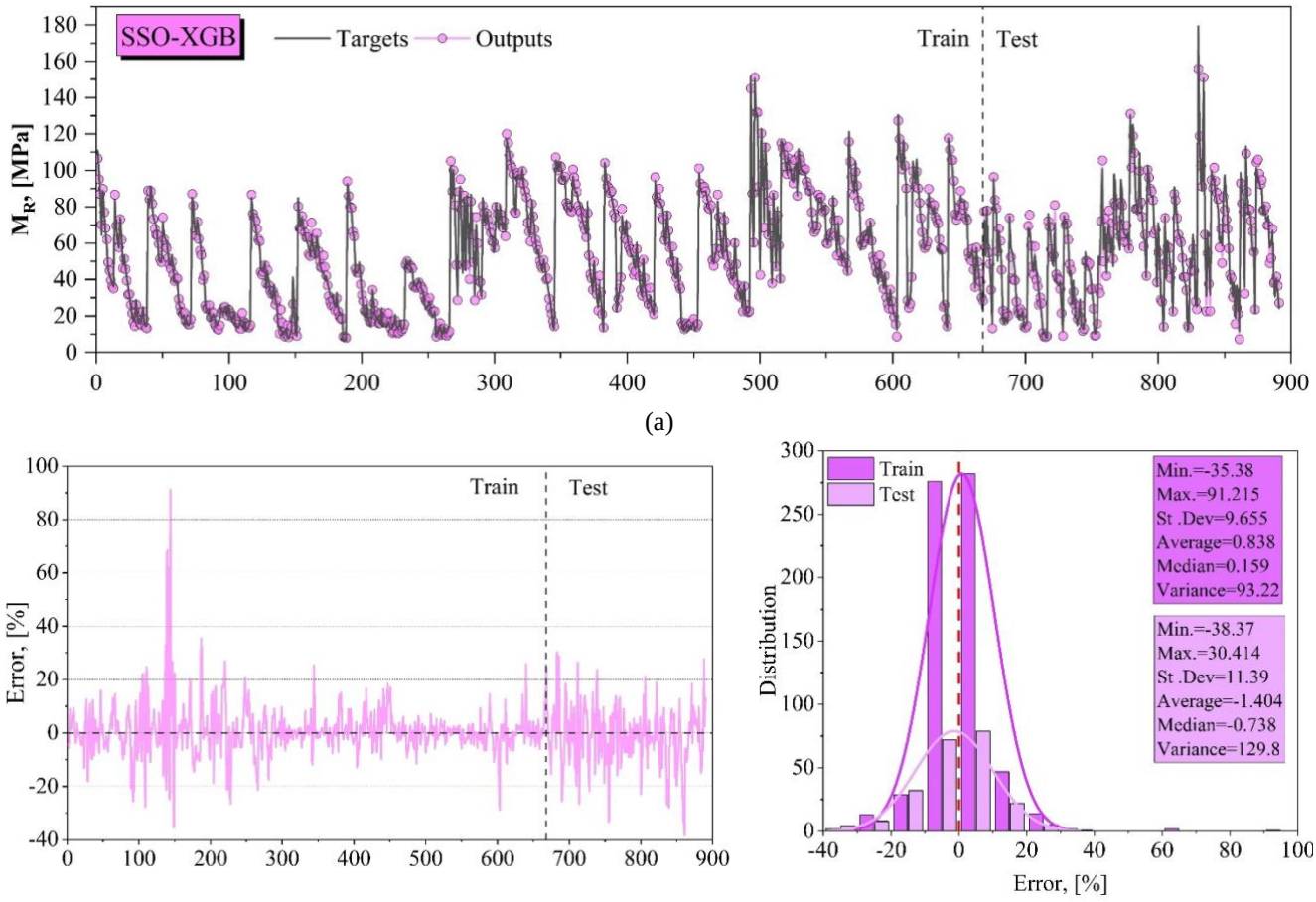

Fig. 16. Results of the developed SSO-XGB model in predicting M_R

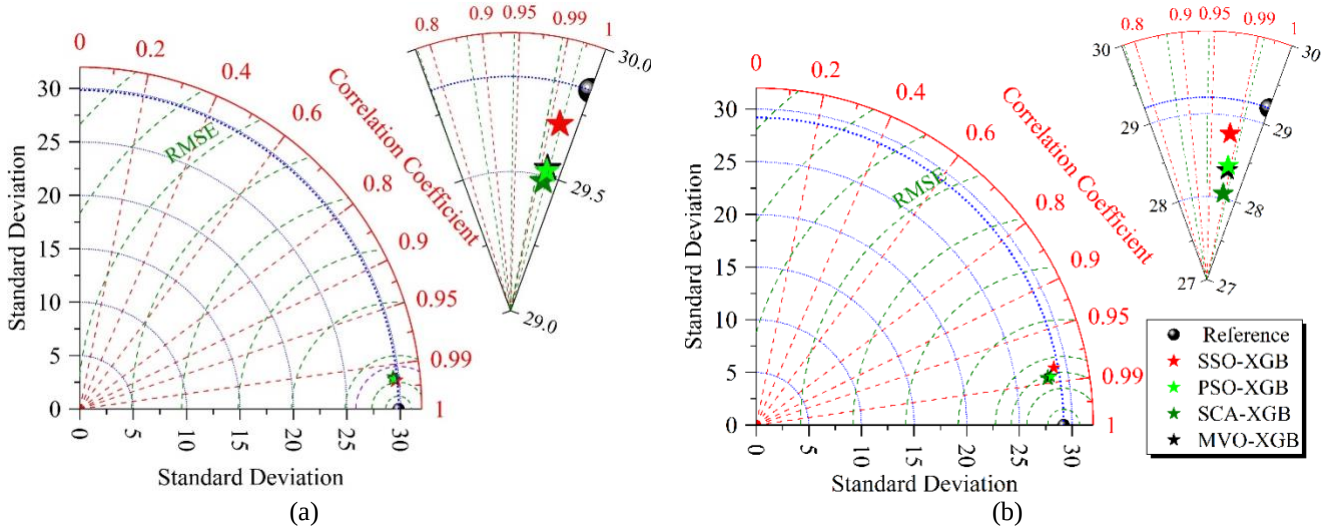

Fig. 17. Comparison of Models' performance in Taylor diagram: a) Training phase, b) Testing phase